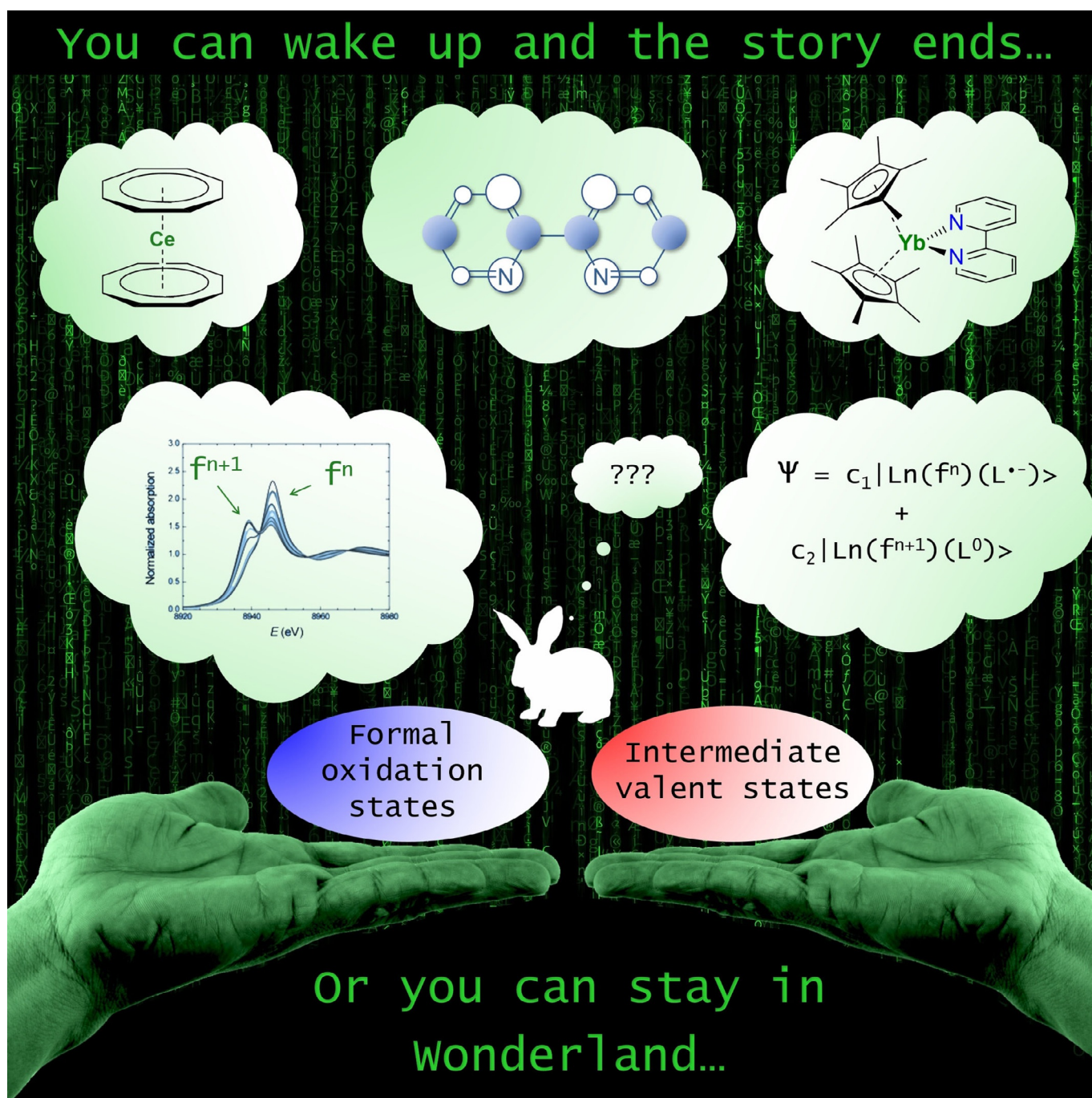


Lanthanide Complexes

Intermediate Valence States in Lanthanide Compounds

Maxime Tricoire, Nolwenn Mahieu, Thomas Simler,* and Grégory Nocton*[a]

In memory of Prof. Richard A. Andersen

Abstract: Over more than 50 years, intermediate valence states in lanthanide compounds have often resulted in unexpected or puzzling spectroscopic and magnetic properties. Such experimental singularities could not be rationalised until new theoretical models involving multiconfigurational electronic ground states were established. In this minireview, the different singularities that have been observed among

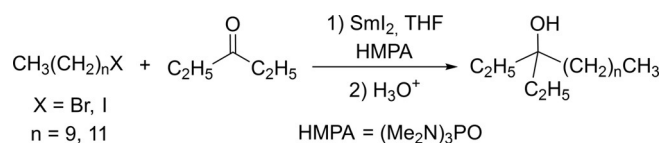
lanthanide complexes are highlighted, the models used to rationalise them are detailed and how such electronic effects may be adjusted depending on energy and symmetry considerations is considered. Understanding and tuning the ground-state multiconfigurational behaviour in lanthanide complexes may open new doors to modular and unusual reactivities.

1. Introduction

The chemistry of lanthanide compounds finds a significant number of direct applications especially because of their important and specific optical and magnetic behaviour.^[1–7] The industry of rare earth elements produces strong magnets for data storage or electrical devices, optics for health and technology and also many materials and molecular complexes for catalysis—including photocatalysis, polymerisation and reductive chemistry.^[7–9] The physical properties of these species are strongly correlated to high spin-orbit coupling, which is due to relativistic effects in these relatively heavy elements. Thus, the appropriate quantum number is *J* and the ligand field is significantly smaller than the spin-orbit coupling. Moreover, the weak screening of f-electrons leads to contraction of the ionic radius when the atomic number increases. Another important physical property of the f-orbitals is their core nature in the shell. As a consequence, the surrounding ligands often do not play a large role in the energy of those core f-orbitals; minimal spatial overlap occurs between the f-orbitals and the Lewis bases coordinated to the lanthanide ions.^[10] Finally, except for cerium and europium, the principal formal oxidation state of these elements is trivalent. These textbook properties have, however, been challenged in recent years, in particular as several groups have been able to synthesise divalent complexes for all the lanthanide series (except for the radioactive Pm) with adapted ligand environments,^[11–18] but also with the number of examples of high-valent molecular compounds increasing rapidly.^[19–23] The multiple occurrences of these unusual oxidation states ask the question as to whether the physical properties discussed above and the models used to understand them are still valid. If any unexpected properties appear

in those unusual oxidation state species, it would then indicate that some aspects of the metal–ligand bonding nature might have been underestimated. In low-valent species, the participation of the empty 5d-manifold is in question,^[18,24] as is the role of strongly donating ligands in high-valent species.^[23,25] This observation notably tends to indicate that the choice of the ligand should not be dictated only by the sterics but also by symmetry and energetic considerations, which is an important paradigm shift in lanthanide chemistry.

In low-valent chemistry, the question of a possible electronic contribution of the ligand to the reduction potential appeared with the important work of Flowers and co-workers on the role of hexamethylphosphoramide (HMPA) addition in reductive chemistry with divalent samarium (Scheme 1).^[26–27]





Scheme 1. Samarium Barbier reaction as described by Flowers and co-workers (adapted from Ref. [27]).

Procter, Maron and co-workers followed this by examining the role of water as solvent in these reactions.^[28] Aside from the study of organic transformations, in typical synthetic low-valent chemistry, the ligands were often chosen for solubility and stability reasons; the bulkier the ligand, the more stable the complex, even with non-classical divalent lanthanides.^[13] The use of elaborated ligands to stabilise low-valent lanthanides also generated important information on the influence of the ligand electronics in the reduction reactivity; if most samarium complexes do not reduce N₂ or CO, decamethyl samarocene is thought to do so,^[29,30] and is capable as well of reducing pyridine to form a C–C coupled dimeric complex whereas the same reactivity was not observed with a similar phospholyl ligand,^[31] presumably because of a redox potential modulation induced by the ligand. The ligand–metal pair thus takes importance and several electronic effects in the reduction reactivity have been noticed. For instance, a reversible C–C bond coupling was observed,^[32,33] the free enthalpy of which can be correlated to the redox potential of the reductive lanthanide fragment versus that of the ligand.

This proposition of an adapted energy for the ligand–lanthanide pair is extremely important because it is related to the

[a] M. Tricoire, N. Mahieu, Dr. T. Simler, Dr. G. Nocton
 LCM, CNRS
 Ecole polytechnique
 Institut Polytechnique de Paris
 Route de Saclay, 91128 Palaiseau, cedex (France)
 E-mail: thomas.simler@polytechnique.edu
 gregory.nocton@polytechnique.edu

 The ORCID identification number(s) for the author(s) of this article can be found under:
<https://doi.org/10.1002/chem.202004735>.

 © 2020 The Authors. Chemistry - A European Journal published by Wiley-VCH GmbH. This is an open access article under the terms of the Creative Commons Attribution Non-Commercial License, which permits use, distribution and reproduction in any medium, provided the original work is properly cited and is not used for commercial purposes.

theory of covalency in metal complexes.^[34] If an immediate relation with covalency is drawn in the case of a strong overlap between the ligand and the metal orbitals (nephelauxetic effect), the energy gap between them is often neglected. Given that the 4f electrons do not mix to a great extent with ligand orbitals of hard donors—such as oxygen, carbon and nitrogen—most lanthanide complexes are expected to present a purely ionic bonding with no covalency (Figure 1).^[35–37]

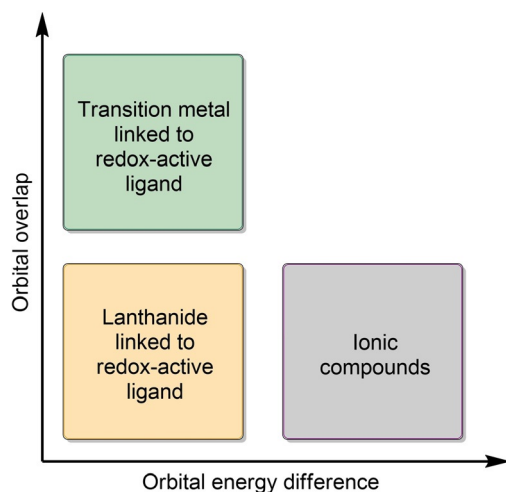


Figure 1. Orbital overlap versus orbital energy difference plot and the related compound categories (adapted from Ref. [38]).

However, when the ligand and the metal both possess similar energies, even with a very little overlap, the electron(s), statistically, have similar probabilities of being found on one or the other site. This situation leads to multiple possible configurations, in which the redox state of the metal is different: the metal and the ligand share electrons even with little overlap between the respective orbitals. This situation of multiple configurations is also known in transition-metal complexes when the orbitals are almost orthogonal, resulting in a small-to-zero overlap extent. Notably, the Wieghardt group and some of us have reported transition-metal complexes with multiple configurations, in which the corresponding redox states are different.^[39–46]

Thus, in lanthanide complexes, when the ligand orbitals and the lanthanide ion are of similar energy, these situations of multiple configurations with different redox states (of both the ligand and the metal ion) can occur, leading to a disturbance in their physical properties. The formal oxidation state is therefore not suitable anymore, as neither one nor the other value is appropriate. The valence is rather intermediate, as discussed in the field by the pioneers, Dolg, Fulde, Maron and Andersen.^[47–51] Indeed, the computation of multiple states of similar energy requires cautious choices of the methods used and, although density-based methods usually lead to fast analyses, in most cases, it solely points out delocalised density over the metal and ligand orbitals but does not reproduce nor explain the abnormal spectroscopic signatures that were observed. In this area, Field considered in the 1980s the computation of di-

atomic molecules of lanthanides for the better understanding of their non-trivial spectroscopic properties, especially arising from low-lying electronic states, and introduced the concept of “super-configurations”.^[52] At the time, if the key theoretical milestones of modern theoretical wave-function-based methodologies^[53,54] and DFT calculations^[55,56] were known, the large number of electrons in f-element complexes rendered the task

Maxime Tricoire did his studies at Ecole Normale Supérieure (ENS) in Paris. After getting his master's degree from Université Pierre et Marie Curie in Paris (now Sorbonne Université) in 2017, he joined Dr. G. Nocton's group at Ecole polytechnique in 2018 for his Ph.D. project involving lanthanides, redox-active ligands and transition metals.



Nolwenn Mahieu started her studies at the Ecole Normale Supérieure (ENS) Paris-Saclay in 2016. After a stay in Pr. E.J. Schelter's group at the university of Pennsylvania working on imido-thorium complexes, she graduated in 2020 with a master in molecular chemistry from ENS Paris-Saclay. She then joined Dr. G. Nocton's group at Ecole polytechnique for her Ph.D. studies on the synthesis of organolanthanide complexes.



Thomas Simler graduated in 2012 from the Ecole Normale Supérieure in Lyon. He received his Ph.D. in 2016 from the Université de Strasbourg working on functionalised NHC and pincer complexes with Dr. P. Braunstein and Dr. A.A. Danopoulos. He then joined the group of Prof. P.W. Roesky at the Karlsruhe Institute of Technology for a first postdoctoral stay supported by an Humboldt fellowship. Since 2019, he is working as postdoc in the group of Dr. G. Nocton at Ecole polytechnique.



Grégory Nocton was born in Reims, France in 1983. After a master of science at the Universities of Reims and Grenoble (2006), he obtained his Ph.D. in 2009 in Grenoble with Prof. Marinella Mazzanti, working on redox reactivity of uranium. He then joined UC Berkeley for two years working with Prof. R.A. Andersen and was appointed CNRS researcher in 2011 at Ecole polytechnique. He obtained the bronze medal of CNRS in 2016 and he is also associate professor at Ecole polytechnique since 2017.



rather difficult. Similarly, when multiconfigurational methods^[57,58] appeared, such as multiconfiguration Hartree–Fock/self-consistent field (MCHF/SCF), configuration interaction (CI) methods, many-body perturbation theory (MBPT) and coupled-clusters (CC),^[59–62] only a few studies were attempted with lanthanide complexes. It is only in the late 1980s that Fulde et al. developed the foundations of the proper understanding of the theoretical approach of such fluctuating systems,^[47,63] notably rationalising the formation of open-shell singlets and/or low-lying multiplet states by using the interaction between two partners (metal–metal or ligand–metal). This approach provided a possible explanation for several experimental observations based on the analogy with the Kondo singlet-state known in solid-state physics.^[64,65]

The present review gathers the historical basis that allowed the development of intermediate valence in lanthanide compounds over more than 50 years of spectroscopic singularities and many computational studies. It opens with a rational basis of the symmetry and energetic considerations that can lead to the prediction of these events and, importantly, describes how they may relate to the reactivity of the complexes (Figure 2). With the abundance of low- and high-valent lanthanide compounds isolated in the last few years, this topic is likely to receive broad and increasing attention.

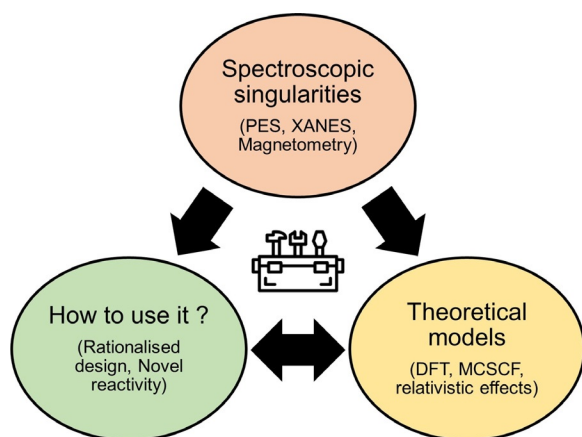


Figure 2. Intermediate valence and multiconfigurational ground states in lanthanide compounds: from spectroscopic singularities to the development of new theoretical models and the application in novel reactivity.

2. Spectroscopic Singularities

In the 1950s, Wilkinson and Birmingham reported the synthesis of a series of $[\text{LnCp}_3]$ ($\text{Cp} = \eta^5\text{-C}_5\text{H}_5$) complexes (Table 1).^[66–68] The latter were obtained as crystalline solids after sublimation under reduced pressure at high temperatures. The ionic nature of the new compounds was evidenced by their reactivity towards ferrous chloride (FeCl_2), resulting in an instantaneous ligand exchange reaction and quantitative formation of ferrocene, $[\text{FeCp}_2]$. Such an ionic nature would result from a dominant electrostatic interaction between the highly electropositive metal centres and the Cp rings with well-separated charges.^[69] The effective magnetic moments for the $[\text{LnCp}_3]$ com-

Table 1. General structure of the $[\text{LnCp}_3]$ complexes and magnetic data at room temperature (295–300 K) for selected compounds.

Ln	Electronic configuration of metal ion	Ground state of metal ion	Exptl. $\mu_{\text{eff}}^{\text{[a]}}$	Calcd. $\mu_{\text{eff}}^{\text{[b]}}$
Ce ^{III}	4f ¹	² F _{5/2}	2.46	2.54
Eu ^{III}	4f ⁶	⁷ F ₀	3.74 ^[c]	3.40–3.61 ^[e]
Yb ^{III}	4f ¹³	² F _{7/2}	4.00	4.54
Lu ^{III}	4f ¹⁴	¹ S ₀	diamagnetic	

[a] Values from Ref. [67], unless otherwise stated. [b] Theoretical values in the free-ion approximation. [c] Value from Ref. [71]. [d] Value for the mono-THF adduct, calculated with the data from Ref. [72]. [e] Non-magnetic ground state but presence of thermally populated magnetic excited states,^[73] estimated values at room temperature from Ref. [74].

plexes were determined experimentally. The overall values were in good agreement with the free-ion values, to the exception of one noticeable discrepancy: the reported magnetic moment of $[\text{YbCp}_3]$, $4.0 \mu_{\text{B}}$,^[67] differs from the expected value of $4.5 \mu_{\text{B}}$ for an Yb^{III} ion in a ²F_{7/2} ground state and is significantly lower than the experimental values for other typical Yb^{III} coordination compounds.^[70]

Following this seminal report, in-depth analysis of the electronic and magnetic properties of several $[\text{LnCp}_3]$ complexes or other lanthanide compounds have been carried out to evaluate and quantify covalency in such compounds, and revealed other spectroscopic singularities that are gathered in this sub-section.

2.1. YbCp₃

Gas-phase photoelectron spectra were recorded for a series of $[\text{LnCp}_3]$ ($\text{Ln} = \text{Ce}, \text{Pr}, \text{Nd}, \text{Sm}, \text{Yb}, \text{Lu}$) complexes using variable photon energy.^[75–79] Photoelectron (PE) spectroscopy has especially proved to be a valuable technique to assess the molecular electronic structure of lanthanide complexes and identify ion states resulting from 4f ionisation. In the case of a lanthanide complex featuring a 4fⁿ ground-state configuration, the spectrum obtained upon ionisation of a 4f valence electron gives information on the ground and excited states of the corresponding 4f^{n–1} cation.

The PE spectrum of $[\text{LuCp}_3]$ ^[80] can be readily interpreted: upon f-electron ionisation from the closed 4f¹⁴ shell of Lu³⁺, two bands were observed and assigned to the ²F_{7/2} and ²F_{5/2} ion states associated with the 4f¹³ configuration of Lu⁴⁺.^[77] In the case of $[\text{YbCp}_3]$, a more complex spectrum was obtained with signals arising from both the 4f¹² and 4f¹³ final-state configurations. An important question is whether the presence of both signals is the result of initial or final-state effects, that is, if the multiconfigurational character of the $[\text{YbCp}_3]^+$ cation ob-

tained upon ionisation does reflect (or not) that of the corresponding neutral $[\text{YbCp}_3]$ complex. The fact that ytterbium readily forms divalent complexes supports the idea of an initial-state effect, that is, contributions from both $\text{Yb}^{\text{III}} 4f^{13}$ and $\text{Yb}^{\text{II}} 4f^{14}$ configurations in the ground state of $[\text{YbCp}_3]$. More precisely, the mixed-configuration ground state corresponds to the superposition of a Lf^{13} configuration and a $\underline{\text{L}}f^{14}$ charge-transfer configuration involving electronic transfer from the Cp ring to the Yb^{3+} ion, where L represents a full ligand shell (the ligand molecular orbitals collectively) and $\underline{\text{L}}$ a hole in that shell.^[77] Careful analysis of the intensities of the bands associated with the two ion states allowed a determination of the relative contributions of the two configurations in the ground state.^[78] The $\text{Yb}^{\text{III}} \text{Lf}^{13}$ configuration was determined to account for 88% of the density in the ground state whereas the $\text{Yb}^{\text{II}} \underline{\text{L}}f^{14}$ charge-transfer configuration contributes 12%. Independent estimations of the relative weights of the two configurations were also obtained by thorough EPR investigations.^[78] Analysis of the ^{13}C hyperfine coupling, as determined by HYS-CORE (hyperfine sublevel correlation)^[81] pulsed EPR experiments, revealed an increase of $12.6 \pm 0.9\%$ in the spin density on the ^{13}C atoms of the Cp rings. In parallel, a decrease in the ^{171}Yb hyperfine coupling interaction was observed compared with a series of standard Yb^{3+} compounds, indicating a reduced spin density in the 4f shell of the ytterbium atom. The observed $\text{Yb} \rightarrow \text{Cp}$ spin transfer is linked to the $\text{Cp} \rightarrow \text{Yb}$ charge transfer associated with the $\underline{\text{L}}f^{14}$ configuration. Finally, the relative weights of the two configurations could also be estimated by analysis of the principal values of the g -tensor and the axial anisotropy, which is partially quenched owing to the charge-transfer configuration.^[78]

The presence of two configurations in the ground state of $[\text{YbCp}_3]$ is expected to have an influence on the magnetic susceptibility of the compound. Therefore, magnetic studies were performed in the solid state in the range 2–305 K.^[77] Above 20 K, a Curie behaviour was observed over the entire temperature range with an associated magnetic moment of $3.53 \mu_{\text{B}}$.^[77] This low magnetic moment compared with that of typical Yb^{III} complexes can be explained if the ground-state wavefunction includes a $\underline{\text{L}}f^{14}$ charge-transfer contribution, with a largely quenched orbital angular momentum. A slightly lower value for the magnetic moment ($3.33 \mu_{\text{B}}$) was derived from EPR measurements in frozen solution. The higher value obtained from solid-state magnetic measurements can be explained by a higher dielectric constant in the solid state, which stabilises the more polar Lf^{13} configuration and reduces the weight of the $\underline{\text{L}}f^{14}$ charge-transfer contribution in the solid state.^[78] As a result of the Curie behaviour, the magnetic moment showed almost no dependence on the temperature in the range 20–305 K, which can be explained by a negligible thermal population at 300 K of high-lying excited states (higher than 1000 cm^{-1}).^[77] Below 20 K, substantial departure from the Curie behaviour was observed, which may be interpreted as a structural phase change occurring at a temperature of 20 K.^[77] As a result of this phase change, the relative weights of the f^{13} and f^{14} configurations in the ground state are likely to be perturbed, leading to different magnetic properties.

Anomalous features were also observed in the electronic spectra of $[\text{YbCp}_3]$. Such spectra, in the solid state^[82] and in solution,^[83] had already been reported in 1967 and 1983, respectively, but remained largely uninterpreted until more recent work by Denning et al. in 2011.^[78] In the visible/near IR spectrum of $[\text{YbCp}_3]$, the f - f region is highly anomalous compared with that of conventional Yb^{3+} compounds, such as, for example, $[\text{Cp}^*_2\text{Yb}(\text{L})^+(\text{X})^-]$ ($\text{L} = 1,10\text{-phenanthroline (phen)}$ or $2,2'\text{-bipyridine (bipy)}$; $\text{X} = \text{I}$ or PF_6 ; see also below, section 2.7).^[84,85] Indeed, f - f transitions in lanthanide compounds (similarly to d - d transitions for transition-metal complexes) are parity forbidden on the basis of the selection rules. The intensities of the corresponding bands were found to be 20 to 50 times larger than those for typical Yb^{3+} compounds and vibronic structures associated with f - f transitions spanned a much larger energy range (ca. 2000 cm^{-1} compared with $597 \pm 185 \text{ cm}^{-1}$). Such anomalous features can be explained by charge-transfer transitions supporting a configuration interaction in the ground state.^[78]

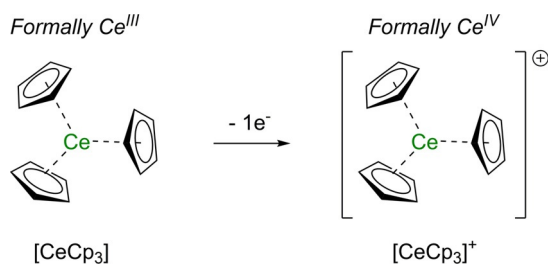
Although routine DFT calculations clearly indicated delocalisation of the spin density away from the Yb atom, they were not appropriate to evaluate the residual spin density on Yb. Using different DFT methods, large differences in the spin density values were obtained. Yet, such computational methods were still useful to give certain insights in the electronic structure, such as the relative orbital energies, and rationalise the experimental electronic and EPR spectra.^[78]

2.2. EuCp_3

The involvement of a $\text{Cp} \rightarrow \text{Ln}$ charge-transfer contribution similar to that in $[\text{YbCp}_3]$ is also expected in the more easily reduced Eu^{III} analogue. Indeed, the $\text{Ln}^{3+}/\text{Ln}^{2+}$ redox potentials versus NHE (NHE = normal hydrogen electrode) are -0.35 V and -1.15 V for Eu and Yb, respectively.^[86] In the case of europium compounds, ^{151}Eu Mössbauer spectroscopy is a useful technique to probe the electronic properties at the europium nucleus. The ^{151}Eu isomer shift strongly depends on the oxidation state of the europium ion whereas the quadrupole interaction gives information about the symmetry of the environment at the metal centre.^[87] In the ^{151}Eu Mössbauer spectrum of $[\text{EuCp}_3(\text{THF})]$, an unusual isomer shift lying between the typical values for Eu^{II} and Eu^{III} complexes was observed, together with a large negative quadrupole interaction, which is also unusual for europium organometallic compounds.^[88] To explain such features, a strong interaction between the Eu 4f orbitals and the three Cp ligands, resulting in the transfer of approximately 0.14 electrons from the ligand sphere to the metal, was suggested.^[88]

2.3. CeCp_3

Among $[\text{LnCp}_3]$ complexes, the cerium analogue was reported to be the most reactive towards oxidation by traces of air, which can be traced back to the easy oxidation of the Ce^{III} centre to Ce^{IV} (Scheme 2).^[66,67] The reported magnetic moment of $[\text{CeCp}_3]$ ($2.46 \mu_{\text{B}}$) at room temperature is consistent with



Scheme 2. Structures of the formally Ce^{III} complex $[\text{CeCp}_3]$ and its related Ce^{IV} cation $[\text{CeCp}_3]^+$.

that expected for an unperturbed $\text{Ce}^{\text{III}} 4f^1$ configuration with a $^2F_{5/2}$ ground state ($2.54 \mu_B$, Table 1).^[67] Insights into the electronic ground state of $[\text{CeCp}_3]$ and in the optical transition energies of this $4f^1$ complex were given by non-relativistic and relativistic DFT calculations.^[89] Analysis of the symmetry of the orbitals revealed that the C_{3v} ligand environment observed in $[\text{CeCp}_3]$ is particularly adapted for f-block elements featuring valence f-orbitals, in contrast to transition metals that possess valence d-orbitals. Although the incorporation of relativity into the calculations only had minor effects on the largely ligand-based molecular orbitals (MOs), it did affect the energies of metal-localised atomic orbitals (AOs). Indeed, relativistic effects destabilise the f-orbitals, bringing the Ce 4f and 5d orbitals closer in energy, which has a direct influence on the electronic absorption spectrum. Although both non-relativistic and relativistic calculations predicted a $4f^1$ ground-state configuration for $[\text{CeCp}_3]$, the inclusion of relativity led to a $6d^1$ ground state for the heavier actinide analogue $[\text{ThCp}_3]$. The calculated electronic absorption spectrum of $[\text{CeCp}_3]$ revealed weak $f \rightarrow f$ transitions with a more intense low-lying $f \rightarrow d$ transition.^[89]

The electronic structures of the neutral complex and of its cationic form $[\text{CeCp}_3]^+$ were further investigated by variable photon energy photoelectron (PE) spectroscopy in the gas phase.^[75] Upon ionisation of the single f-electron of $[\text{CeCp}_3]$, a simple orbital model would predict only one possible ion state for the corresponding $4f^0$ $[\text{CeCp}_3]^+$ cation, that is, only one photoelectron band in the PE spectrum. However, two bands separated by a large energy gap (3.2 eV) and associated with two different final states were observed.^[75] It should be noted that the occurrence of two signals associated with f-ionisation had already been reported in the photoemission spectra of solid inorganic Ce compounds.^[90–92] In the PE spectrum of $[\text{CeCp}_3]$, the lower energy state associated with the first PE band corresponds to the ground state of the gas-phase $[\text{CeCp}_3]^+$ cation. Its electronic structure was rationalised in terms of an interaction between two different electronic configurations.^[75] Further studies revealed that, although the ground state of $[\text{CeCp}_3]^+$ does not possess a Ce-localised f-electron, it has significant f-density arising from population of natural orbitals (NOs) with f-character.^[76] The higher energy band in the PE spectrum also arises from f-ionisation and is associated with an excited state of $[\text{CeCp}_3]^+$. This excited state features significant Ce5d population owing to intramolecular Cp \rightarrow Ce5d charge transfer occurring upon f-ionisation. Insights into the electronic structure of the different states of $[\text{CeCp}_3]^+$

was provided by ab initio calculations using the complete active space self-consistent field (CASSCF)^[93]/complete active-space second-order perturbation theory (CASPT2) approach.^[76] The CASPT2 methodology includes perturbations by additional corrections for dynamic correlation.^[94]

However, electronic configurations involving canonical CASSCF orbitals were found not to reliably describe the electronic structures of the ground and excited states of $[\text{CeCp}_3]^+$. Indeed, the weights of these configurations were highly influenced by the number of states included in the state-averaged (SA) CASSCF calculation (see discussion below on cerocene). The NOs and their occupations (NOOs) are specific to each state and are more informative. They are computed from the reduced density matrix of each state and not from the state-averaged matrix, the latter being used to produce pseudo-NOs in CASSCF/CASPT2 calculations. The f-electron occupancy can then be derived from the NOOs and their f-coefficients for all the active space orbitals. A deviation >0.1 from an integer value for the NOOs ensures the presence of a multiconfigurational state. As a result, in the $[\text{CeCp}_3]^+$ cation, several configurations were found to compose the wavefunction, resulting in an intermediate-valent ground state. The same conclusion was obtained for the excited states involved in the second PE band. Yet, as no NO is purely f-based in the electronic ground state of $[\text{CeCp}_3]^+$, the latter does not possess any metal-localised 4f electron, which supports the description of this cation as formally Ce^{IV} . The significant f-density on the metal centre, similar to that in the formally Ce^{III} $[\text{CeCp}_3]$, is due to population of delocalised NOs with f-character.^[76] This conclusion highlights the very core of the semantic issue arising in these kind of systems. How to qualify a Ln ion that shows properties from a different oxidation state than its formal one? The theoretical model supports intermediate valence as it uses multiconfigurational states to define the system but these states may bear no fundamental characteristics of one or the other oxidation state involved (i.e., no pure f-orbital localised electron in this case).

2.4. Cerocene and derivatives

Aside from the $[\text{LnCp}_3]$ complexes, the electronic structure of cerocene, $[\text{Ce}(\text{Cot})_2]$ (Cot = $\eta^8\text{-C}_8\text{H}_8$; Figure 3), has been the subject of a great deal of research from both experimental and theoretical points of view.

The successful synthesis of cerocene was first reported in 1976 by Cesca and co-workers, by reaction of $[\text{Ce}(\text{O}i\text{Pr})_4]$ with $[\text{AlEt}_3]$ in the presence of excess cyclooctatetraene (Cot).^[95] Cer-

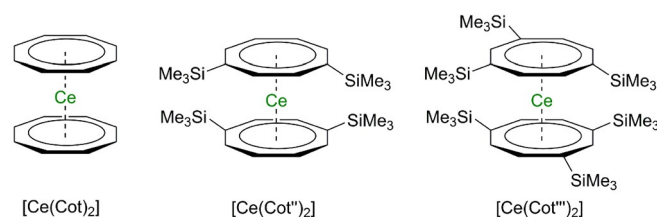


Figure 3. Structure of cerocene and its trimethylsilyl-substituted analogues.

ocene combines a strong reducing agent (the Cot^{2-} dianion) and a strong oxidising agent (a Ce^{4+} ion). Alternative and higher-purity syntheses of $[\text{Ce}(\text{Cot})_2]^{[96,97]}$ and of several substituted cerocenes have also been described.^[98,99] In such complexes, the distance between the ring centroid and the Ce metal centre is approximately 1.97 Å, which is approximately 0.10 Å shorter than the corresponding distance in the Ce^{III} $[\text{Ce}(\text{Cot})_2]$ diglyme salt.^[100] Such a shortening is consistent with the smaller ionic radius of the Ce^{4+} cation compared with that of the Ce^{3+} cation.^[101] In addition, electrochemical studies and the apparent diamagnetism of cerocene were further pointing to a formal Ce^{IV} complex.

In the gas-phase PE spectrum of $[\text{Ce}(\text{Cot})_2]$, no clear sign of f-electron ionisation was observed, also supporting a $4f^0$ configuration, that is, a +IV oxidation state for the metal centre, similarly to the situation encountered in the heavier 5f thorium analogue.^[102] In the UV/Vis spectrum, strong absorption bands in the visible region at 469 nm (ϵ ca. 8000) with a shoulder at 570 nm (ϵ ca. 1000) were assigned to ligand-to-metal charge-transfer transitions. The substituted cerocene $[\text{Ce}(\text{Cot}'')_2]$ ($\text{Cot}'' = 1^8\text{-}1,4\text{-}(\text{Me}_3\text{Si})_2\text{C}_8\text{H}_6$; Figure 3), first reported in 1994 by Edelmann and co-workers, was obtained by oxidation of the Ce^{III} complex $\text{Li}[\text{Ce}(\text{Cot}'')_2]$ with AgI, and isolated as a deep-purple oil.^[99] An alternative synthesis, consisting of the oxidation of $\text{Na}[\text{Ce}(\text{Cot}'')_2]$ with allyl bromide, was described by Streitwieser and co-workers and led to the same compound, $[\text{Ce}(\text{Cot}'')_2]$, isolated as a dark-brown semisolid material.^[96] The UV/Vis spectra of $[\text{Ce}(\text{Cot}'')_2]$ and of other substituted cerocenes ($[\text{Ce}(\text{C}_8\text{H}_7\text{R})_2]$ with $\text{R} = \text{Me}, n\text{Bu}, t\text{Bu}, t\text{BuO}$) were recorded and revealed a maximum absorption band in the region 470–494 nm.^[96,99] This band was first attributed to a ligand-to-metal charge-transfer transition occurring in formal Ce^{IV} complexes,^[96] similarly to the situation in cerocene.^[102] However, further spectroscopic studies on $[\text{Ce}(\text{Cot}'')_2]$ at variable temperatures reported by Amberger et al. were more consistent with a Ce^{III} formulation.^[103] In the luminescence spectrum at low temperature (90 K), two bands were observed with maxima at 14 250 and 17 900 cm^{-1} , which is typical for Ce^{III} complexes, as, for example, $[\text{Li}(\text{THF})_4][\text{Ce}(\text{Cot})_2]$. The separation between the two bands, 3650 cm^{-1} , is, however, bigger than that usually observed in Ce^{III} complexes (typically 1250–1400 cm^{-1}) and is in agreement with the energy separation predicted by calculations corresponding to a $\text{Ce}^{3+}[(\text{Cot})^{1.5-}]_2$ formulation (see below).^[47–49] The authors could nonetheless not totally exclude the possibility that some of the luminescence signals detected a low temperature may arise from Ce^{III} decomposition products under laser irradiation.^[103]

X-ray absorption near-edge structure (XANES) spectroscopy studies have been carried out to further investigate the oxidation state of Ce in cerocene and its substituted analogues.^[97,104–106] Through the exposure to high-energy X-rays, core electrons are excited into empty or singly occupied valence orbitals of the metal complex (Figure 4). XANES has been recognised as a useful tool to determine the oxidation state of an atom and has been used to evaluate the degree of f-orbital participation in the bonding of lanthanide and actinide compounds.^[107,108] The absorption is measured below and above a

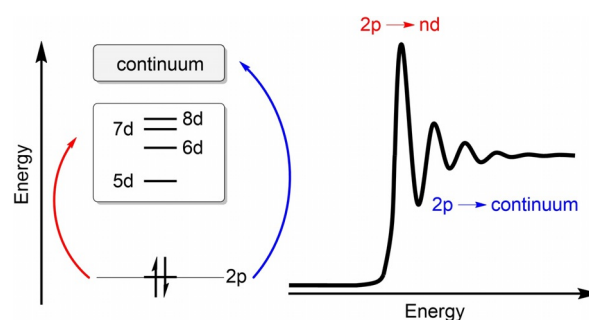


Figure 4. Schematic representation of L_3 -edge XANES transitions and their origin. Adapted from Ref. [24].

characteristic X-ray elemental edge. For example, for metal ions, K-, L-, or M-edge X-ray absorption spectroscopy (XAS) has been employed. Some reports focused on ligand K-edge XAS studies on the atoms directly bound to Ln centres to investigate metal/ligand orbital mixing and covalency in lanthanide compounds.^[23,106,109–111] These different XAS techniques differ by the energy of the transitions involved. Whereas lanthanide K-edge XAS involves high-energy excitations of metal 1s electrons to empty orbitals of p character, lanthanide L_3 -edge XANES studies probe transitions between Ln2p orbitals and unoccupied states of 5d character (i.e., transitions from a $2p^6 4f^n 5d^0$ to a $2p^5 4f^n 5d^1$ electronic state where n corresponds to the number of f-electrons in the ground state).^[24] The energies of the transitions are related to the ground-state $4f^n$ occupation and the effective nuclear charge on the lanthanide ion.

Recently, lanthanide $M_{5,4}$ -edge XAS studies, which involve transitions from core-level 3d electrons to empty 4f orbitals, that is, transitions from $3d^{10} 4f^n$ to $3d^9 4f^{n+1}$ configurations, have been employed to probe 4f valency in lanthanide ions.^[24,106,109,111] The energy at which the absorption edge occurs is linked to the metal oxidation state or f-occupancy in intermediate valence systems. In Ce^{III} complexes, the presence of only one initial state with a configuration $L2p^6 4f^1$ (L corresponding to the orbitals of the ligand) results in a single final state of $L2p^5 4f^1 5d^1$ configuration after L-edge XAS irradiation.

Formal Ce^{IV} compounds, and more generally Ln^{IV} compounds, usually feature a superposition of Lf^0 and Lf^1 (L is a ligand hole) configurations in their ground states. It is, for example, the case in CeO_2 , which is generally considered a strongly mixed-valent compound,^[111–115] although its electronic ground state is still controversial.^[116]

In the corresponding XAS spectra, the white line usually displays multiple peaks, typically in the shape of a white line doublet, owing to contributions of the different configurations in the final state. Quantitative analysis of the multiple features observed in the core-level X-ray photoemission (XPS) spectrum of CeO_2 led to similar conclusions, supporting a mixture of $L4f^0$ and $L4f^1$ configurations in the ground state.^[112] However, the physical origin and the interpretation of the white line doublet in Ln XAS measurements is still under debate and the XPS core final states are different from the XANES final states.^[113] The presence of contributions from both configurations could be the result of either a multiconfigurational ground-state (i.e., ini-

tial-state effects) or final-state effects.^[106,109,111] Final-state effects would support the presence of a single ground state leading to a doublet feature as the result of transitions to unoccupied 5d states split by the crystal field, or strong perturbation and relaxation effects around the core hole.^[23,113] However, most studies support initial-state effects. Analysis of the XANES data of the substituted cerocenes [Ce(Cot^{''})₂] and [Ce(Cot^{'''})₂] (Cot^{'''} = η⁸-1,3,6-(SiMe₃)₃C₈H₅; Figure 3) revealed K-edge shifts at energies similar to those observed in various Ce³⁺ model compounds, therefore supporting a Ce^{III} oxidation state.^[104] However, the edge energies were slightly shifted (about 4.5 eV) towards a higher oxidation state in comparison with the edge energies of the corresponding alkali metal Ce^{III} adducts. Therefore, XANES data support mixed-valence in substituted cerocenes. The lower electronic density compared with typical Ce^{III} compounds was interpreted as an admixture of Ce^{III} $\underline{L}4f^1$ and Ce^{IV} $L4f^0$ configurations in the ground state of cerocene, as predicted in earlier calculations by Dolg, Fulde and co-workers.^[47–49] Andersen and co-workers reported that, using Ce L₃-edge (rather than Ce K-edge) XAS, a well-defined white line doublet can be observed in formal Ce^{IV} compounds, which allows a more precise estimation of the cerium valence in these compounds.^[105] The high-resolution Ce L₃-edge XANES spectrum of [Ce(Cot)₂] was found to be more consistent with that of a Ce^{III} rather than Ce^{IV} compound, but still displayed some characteristic Ce^{IV} features.^[105] These data were in agreement with earlier Ce K-edge XANES data recorded by Edelstein and co-workers on the substituted cerocenes [Ce(Cot^{''})₂] and [Ce(Cot^{'''})₂].^[104] By fitting the Ce L₃-edge XANES data, the relative contributions of the two configurations can be determined. The f-occupancy, n_f , is defined in Equation (1) where $A_{Ln^{3+}}$ is the intensity of the $\underline{L}2p^{5}4f^{n+1}5d^1$ final-state contribution and $A_{Ln^{4+}}$ that of the $L2p^{5}4f^05d^1$ contribution.

$$n_f = \frac{A_{Ln^{3+}}}{A_{Ln^{3+}} + A_{Ln^{4+}}} \quad (1)$$

For cerocene, the estimated value $n_f = 0.89 \pm 0.03$ supports the calculation predictions of Dolg and co-workers (Figure 5).^[49] No influence of the temperature on the n_f value was observed until 400 K, the temperature at which conversion of [Ce(Cot)₂] to [Ce₂(Cot)₃] begins to occur.^[97] The latter compound, in contrast to [Ce(Cot)₂], is clearly trivalent with $n_f = 1$.

Very recent studies focused on Ce M_{5,4}-edge and carbon K-edge XAS to investigate covalency in [Ce(Cot)₂].^[106] The Ce M_{5,4}-edge XAS data were compared with those obtained by L₃-edge XAS studies for other formally Ce^{IV} ([Ce(Cot)₂], CeO₂,

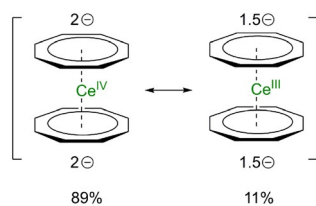


Figure 5. Ce^{IV} and Ce^{III} contributions in cerocene as determined by Andersen and co-workers.^[105]

CeCl₆²⁻) and Ce^{III} ([Ce(Cot)₂][Li(THF)₂] and CeCl₆³⁻) species.^[105,109,111] It should be noted that, compared with L₃-XANES, the intensity ratio between M_{5,4}-XANES final states are quite different and the deduction of ground-state intermediate valence requires a theoretical description of the final states. Although the Ce M_{5,4}-edge XAS spectrum for [Ce(Cot)₂] is more similar to that of formal Ce³⁺ compounds, successful fitting of the data was only possible when including both Ce^{IV} $L3d^{10}4f^0$ and Ce^{III} $\underline{L}3d^{10}4f^1$ initial-state configurations, and the corresponding $\underline{L}3d^94f^1$ and $\underline{L}3d^94f^2$ final-state configurations. A contribution of 51 % of the charge-transfer Ce^{III} configuration to the ground state was established, which is larger than that derived from Ce M_{5,4}-edge XAS data on other formally Ce^{IV} compounds, such as CeCl₆²⁻ (25 %)^[109] or CeO₂ (ca. 44 %).^[111] However, this Ce^{III} contribution to the ground state is much lower than that established by L₃-edge XANES spectroscopy (89 %).^[105]

SQUID magnetic studies revealed that high-purity [Ce(Cot)₂] displays temperature-independent paramagnetism (TIP) in the range 5–300 K, with the magnetic susceptibility χ being slightly positive and temperature independent, which rules out a diamagnetic molecule that would present $\chi_m < 0$.^[97,105] Neumann and Fulde suggested that cerocene may be considered as a molecular analogue of a Kondo singlet.^[47] The Kondo effect is a term derived from the physics of solid-state materials and arises when paramagnetic sites antiferromagnetically couple to conduction electrons, resulting in cancelation of the local magnetic moment.^[64–65,117] The term Kondo singlet means that an open-shell singlet is lying lower in energy than the open-shell triplet, as a result of a mixture of two configurations (in this case the Ce^{III} $\underline{L}f^1$ and Ce^{IV} Lf^0 configurations, with \underline{L} and L corresponding to (Cot^{1.5-})₂ and (Cot²⁻)₂, respectively). In Kondo systems, the triplet state becomes populated by increasing the temperature until the Kondo temperature at which the spins become uncorrelated. In this case, cerocene behaves as a Kondo singlet in the temperature range 5–300 K but decomposes to [Ce₂(Cot)₃] and free Cot before the triplet state begins to be populated.^[97]

Studies of other [Ln(Cot)₂]⁻ complexes by anion photoelectron spectroscopy revealed a pair of prominent peaks in the PE spectra of the middle-range lanthanide (Ln = Sm, Gd, Tb, Dy and Ho) complexes. In contrast, simpler features were observed for the lighter and heavier lanthanide analogues. These results were rationalised in terms of configuration interaction involving both Ln³⁺ and Ln⁴⁺ configurations after photodetachment of one electron.^[118]

As DFT calculations are not well-adapted for these particular systems, they do not properly describe the multiconfigurational character of [Ce(Cot)₂]. Yet, broken-symmetry DFT (B3LYP) calculations seemed to reproduce some aspects of the multiconfigurational character observed by CASSCF calculations and revealed an open-shell singlet ground state resulting from an admixture of singlet and triplet states.^[106] Concerning theoretical models, following the theoretical studies by Rösch and Streitwieser stating that cerocene is at the +IV oxidation state, similarly to uranocene and thorocene,^[119] Neumann and Fulde were the pioneers who opened cerocene's Pandora box in

which was concealed numerous questions about its oxidation state. With the rise of relativistic pseudo-potentials developed for f-elements in the beginning of the 1990s,^[120–123] a huge gap was filled, making possible the study of cerocene with complex MCSCF methods. This led to Dolg's works on the topic, validating the fact that cerocene's ground state had to be considered as intermediate valent with two 1A_g configurations (in D_{8h} symmetry), the open-shell singlet $Ce^{III} \underline{L}f^1$ (or $Ce^{3+}[(Cot)^{1.5-}]_2$) and the closed-shell singlet $Ce^{IV} Lf^0$ (or $Ce^{4+}[(Cot)^{2-}]_2$), which coexist with the Ce^{III}/Ce^{IV} ratio being approximately 83:17. This ratio can be noted $n_f=0.83$ to represent the effective number of f-electrons left on the Ce atom.^[48,49,124] This initial statement that the ground-state wavefunction of cerocene is multiconfigurational was later endorsed by Kerridge. However, suspicions about the Ce^{III} character being predominant led in 2009 to SA-CASSCF^[93] studies coupled with CASPT2^[94] calculations, which resulted in $Ce^{II}/Ce^{III}/Ce^{IV}$ contributions to the wavefunction being 9:23:60, respectively.^[125] One important notion highlighted in this paper is the difference between canonical CASSCF orbitals and natural orbitals. As stated earlier with the $[CeCp_3]$ study, canonical CASSCF MO coefficients are theoretically and numerically relevant but they are subject to large changes upon modulation of the number of states considered in the SA calculation. The more reliable NOs should be considered to evaluate n_f , resulting in a value of $n_f=0.9$ close to that obtained in Dolg's studies and in the experimental ones. Yet, the fact that the NOs remain largely localised on the π -ring system led to the conclusion that this f-density is mostly due to covalency between the Cot and the empty f-orbital on the Ce, which is contradictory with a Ce^{III} definition. A later update using quantum theory of atoms in molecules (QTAIM) topological analyses^[126] derived from CASSCF-CASPT2 level of theory studies confirmed the non-negligible covalency arising from electron sharing between the Cot ring and the Ce ion with a charge of approximately 2.9.^[127] This study enforced the conjecture in which the cerocene ground state is of mixed-valence and closer to the formal oxidation state +IV. The n_f value being close to 1 (0.95 in this study) mainly originates from Cot–Ce covalency and not from the Ce ion itself. The fact that the first excited state is, however, best defined as Ce^{III} from both CASSCF and QTAIM with a similar electronic structure is proposed as another reason why experimental measurements are in better agreement with a +III oxidation state. In 2014, Mooßen and Dolg answered these different statements by using the invariance of the CASSCF wavefunction by a unitary transformation in the orbital space.^[128] Indeed, given this property, by applying the transformation ($a' = a \cos \alpha + b \sin \alpha$) and ($b' = b \cos \alpha - a \sin \alpha$) to any set of starting a and b CASSCF orbitals, it is possible to create a new set of orbitals that will end up representing the very same wavefunction but with a different representation and different contributions (see Figure 6). By incrementing this, Mooßen and Dolg highlighted two extreme cases, on the one hand the purest π and 4f orbitals can be created with $\alpha=25^\circ$ leading to a' being approximately 95% pure π and b' approximately 100% pure 4f. The weights of the configurations to the wavefunction are then 80% for $a'^3b'^1$, 10% for a'^4 and 10% for $a'^2b'^2$, which therefore corre-

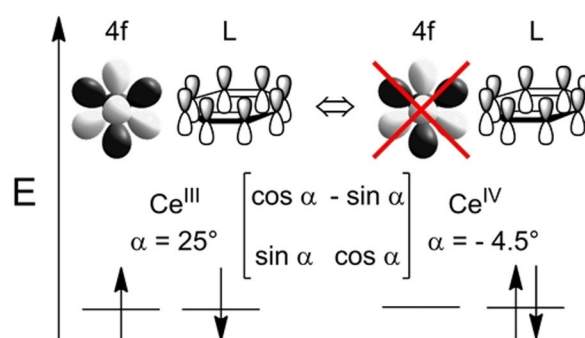


Figure 6. Representation of the two extreme cases of orbital rotation highlighted in Mooßen and Dolg's work of 2014.

sponds to a mostly Ce^{III} intermediate-valent state. On the other hand, the a'^4 configuration contribution is maximised (81%) with $\alpha=-4.5^\circ$, resulting in a' being composed of an 80:20 ratio of $\pi/4f$ orbitals and b' the inverse. As a result, a mostly Ce^{IV} model is obtained but with the resulting orbitals being of mixed character. With these two cases in mind and knowing that an infinite number of combinations may give intermediate results, there is no single best way to describe the formal oxidation state of cerocene. Moreover, all of these combinations are giving a relatively stable n_f close to 1, which concurs relatively well with the experimental value that remains the absolute reference.

These works enlighten us about why intermediate-valent species are so hard to qualify. Dolg stated in his conclusion that the choice between a +III (where a pure 4f electron is present) and a +IV (where the 4f electron density arises from π -4f covalency) oxidation state is "to a certain extent a matter of taste",^[128] which, for a pioneer of the field, is quite meaningful.

2.5. $[Ce(Pn)_2]$ substituted pentalene

Recently, magnetic and spectroscopic studies have focused on the related substituted pentalene analogues of $[Ce(Cot)_2]$, cerium bis(hexamethylpentalene) $[Ce(Pn^*)_2]$ ($Pn^* = \eta^8-Me_6C_8$) and bis(triisopropylsilyl)pentalene $[Ce(Pn'')_2]$ ($Pn'' = \eta^8-(1,4-iPr_3Si)_2C_8H_4$) (Figure 7).^[129,130] In both cases, sharp signals were observed in the 1H and ^{13}C NMR spectra in solution, suggesting diamagnetic molecules, but with several abnormal chemical shifts revealing some paramagnetic character. The unusual

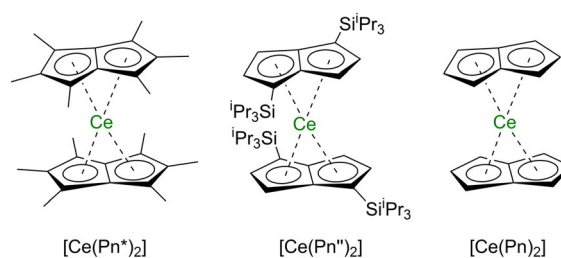


Figure 7. Structures of the different Ce pentalene complexes discussed in this section.

NMR chemical shifts were explained by a strongly “mixed-valent” system with $4f^1$ contributions to the ground state. No appreciable changes in the chemical shifts were observed by variable-temperature NMR studies, implying temperature-independent paramagnetism (TIP). Solid-state magnetic studies revealed a TIP paramagnetism ($(25.0 \pm 0.1) \times 10^{-4}$ and $(4.5 \pm 0.3) \times 10^{-4}$ emu mol $^{-1}$ for $[\text{Ce}(\text{Pn}^*)_2]$ and $[\text{Ce}(\text{Pn}^{\prime\prime})_2]$, respectively) larger than that reported for $[\text{Ce}(\text{Cot})_2]$ ($(1.4 \pm 0.2) \times 10^{-4}$ emu mol $^{-1}$),^[105] which was attributed to smaller HOMO–LUMO gaps in the pentalene complexes.^[129,130] In the UV/Vis spectra, intense absorption bands were detected at 530 nm ($\epsilon = 17\,000$) and 590 nm ($\epsilon = 5000$) for $[\text{Ce}(\text{Pn}^*)_2]$ and $[\text{Ce}(\text{Pn}^{\prime\prime})_2]$, respectively, and were assigned to charge-transfer transitions. The comparative feature in cerocene was observed at 469 nm ($\epsilon = 8000$).^[102]

For both $[\text{Ce}(\text{Pn}^*)_2]$ and $[\text{Ce}(\text{Pn}^{\prime\prime})_2]$ systems, XANES studies revealed intermediate-valent systems, with a formal valence close to Ce^{III} .^[129,130] In the case of $[\text{Ce}(\text{Pn}^*)_2]$, the f -occupancy was determined by fitting the variable-temperature Ce L_3 -edge XANES spectra. A value $n_f = 0.87 \pm 0.05$ close to that in $[\text{Ce}(\text{Cot})_2]$ ($n_f = 0.89 \pm 0.03$) was obtained over the whole temperature range (30–300 K).

DFT calculations were carried out on $[\text{Ce}(\text{Pn}^*)_2]$ and on the model $[\text{Ce}(\text{Pn})_2]$ complex.^[129,130] Although such calculations could not accurately reproduce the observed multiconfigurational ground state, they helped to identify trends in the electronic structure. Contributions from the $\text{Ce}^{\text{IV}} L^0$ and $\text{Ce}^{\text{III}} \underline{L}^1$ configuration were suggested with, in the latter configuration, the f -electron antiferromagnetically coupled to a hole in the ligand shell (\underline{L}) of the same symmetry. Similarly to what has been discussed in the case of cerocene, the *observed* oxidation state, as determined experimentally from XANES data, is closer to Ce^{III} ,^[129] whereas the *formal* oxidation state, derived from the redox potential and the apparent diamagnetism, might be better described as Ce^{IV} .^[130]

Further ab initio calculations were carried out independently by the groups of Kaltsoyannis and Dolg.^[131,132] Using the same methodology as described for the analysis of cerocene (see above),^[125] CASPT2 calculations were performed to determine the electronic ground state of $[\text{Ce}(\text{Pn})_2]$. A particularly large active space correlating 12 electrons in 16 orbitals was used, which allows for occupation of any of the twelve $4f$ and $5d$ levels. Although the symmetry of the ground state, 1A_1 , is in agreement with that obtained by DFT calculations, the multiconfigurational character of the ground state is not accurately described by single-configuration DFT calculations. Analysis of the NOOs derived from CASPT2 calculations led to a calculated f -occupancy $n_f = 0.78 \pm 0.04$ in good agreement with that obtained experimentally ($n_f = 0.87 \pm 0.05$).^[131] These calculations also reproduced the energy of the first band in the UV/Vis spectrum of $[\text{Ce}(\text{Pn}^*)_2]$ with a great accuracy.^[131]

Similarly to the calculations performed on cerocene,^[48,49] Dolg investigated the ground-state electronic structure of $[\text{Ce}(\text{Pn})_2]$ by using advanced CASSCF calculations.^[132] By means of a rotation of the CASSCF natural orbitals, leaving the wavefunction and total energy invariant, a dominant $4f^1\pi^1$ configuration based on nearly pure $\text{Ce}4f$ and ligand π orbitals was ob-

tained. This description is particularly adapted to illustrate the *observed* oxidation state determined experimentally.

These two substituted pentalene cerium complexes are further examples of self-contained Kondo effect in a single molecule.

2.6. Other formally tetravalent lanthanide complexes

Until very recently, no other lanthanide than cerium was reported as a molecular complex in the formal +IV oxidation state.^[23,25] Also, formal Ce^{IV} complexes are not restricted to organometallic complexes and other coordination compounds have been reported (Figure 8).

Mixed valence in cerium bis(phthalocyaninato)cerium $[\text{Ce}(\text{Pc})_2]$ (Figure 8) complexes has been established on the basis of IR and Ce3d XPS spectroscopic data. The cerium centre in these complexes is neither tri- nor tetravalent.^[133] Although similarities in the IR spectra of $[\text{Ce}(\text{Pc})_2]$ and of trivalent $[\text{Ln}(\text{Pc})_2]$ complexes supported a formal Ce^{III} view, careful analysis of the different absorption bands revealed discrepancies with other trivalent $[\text{Ln}(\text{Pc})_2]$ complexes. The absorption band at around 880 cm^{-1} was found to be especially sensitive to the ionic radius of the metal within the lanthanide series, and a linear correlation between the band energy and the metal ionic radius was established. The observed absorption band in $[\text{Ce}(\text{Pc})_2]$ suggested an ionic radius of approximately 1.01 \AA for the Ce centre in $[\text{Ce}(\text{Pc})_2]$, which is intermediate between the ionic radii of Ce^{III} (1.14 \AA) and Ce^{IV} (0.96 \AA) ions in similar coordination environments. Ce3d XPS data further supported a cerium mixed-valent complex with contributions from the $[(\text{Ce}^{4+})(\text{Pc}^{2-})_2]$ and $[(\text{Ce}^{3+})(\text{Pc}^{\cdot-})(\text{Pc}^{2-})]$ configurations in the ground state.^[133] The valence of Ce in a series of tetrapyrrole double-decker complexes bearing (na)phthalocyaninato and porphyrinato ligands with different electronic properties has also been investigated.^[134] The UV/Vis absorption spectra of the substituted Ce phthalocyaninate complexes displayed two ligand absorption bands (the phthalocyanine Q-bands) at un-

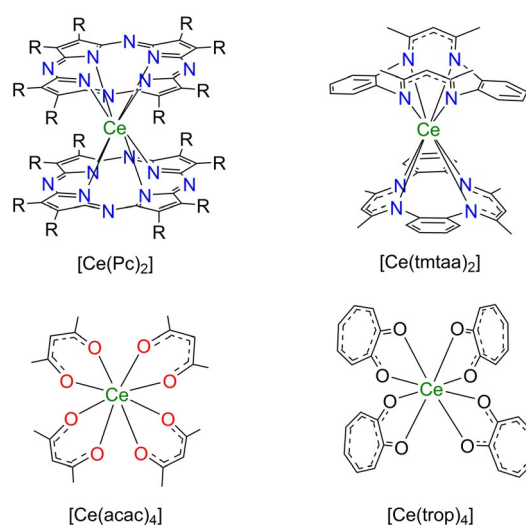


Figure 8. Structures of formal Ce^{IV} complexes bearing non-organometallic ligands.

expected wavelengths. Using a similar approach as above, the ionic radius of the Ce centre was estimated through a linear correlation between the energy of the electronic transition and the lanthanide ionic radius. From this study, the ionic radius of the cerium centre was found to be smaller than that expected for a Ce^{III} ion (1.143 Å) and close to that of Nd^{III} (1.109 Å), suggesting an intermediate valence between +III and +IV for the Ce centre.^[134] Further evidence was given by L₃-edge XANES analyses, which revealed two edge absorption peaks corresponding to the L4^f and L4^f contributions.

Magnetic susceptibility studies on [Ce(tmtaa)₂] (tmtaaH₂ corresponding to tetramethyldibenzotetraaza[14]annulene), cerium tetrakis(acetylacetonate) [Ce(acac)₄] and cerium tetrakis(tropolonate) [Ce(trop)₄] (Figure 8) as a function of temperature have shown that these formally 4^f complexes exhibit temperature-independent paramagnetism (TIP) with low but positive values of χ for the metal centre (after subtraction of the ligand diamagnetic contribution).^[135–137] The small energy difference between the ground state (open-shell singlet) and the first excited state (open-shell triplet) was found to be responsible for the TIP behaviour. In an applied magnetic field, thermal mixing of the two states occurs with a relative population following the Boltzmann distribution, which results in a small net value of the magnetic moment μ_{eff} (in the range 0.1–0.7 μ_{B} at 300 K). The experimental results were therefore not consistent with diamagnetic cerium centres (associated with negative values of χ), which would arise from a single 4^f Ce^{IV} ground-state configuration. Ce L₃-edge XAS studies and ab initio calculations based on multireference wavefunctions further confirmed a Ce^{III} 4^f and Ce^{IV} 4^f multiconfigurational character in the ground states of these complexes. The calculations were performed by using CASSCF/CAS-SDCI methodologies starting with a relatively large active space (four electrons distributed over five orbitals) further reduced to two active electrons. Averaged orbitals of the f^2L^6 , f^1L^7 and f^0L^8 states were used in the calculations. Finally, the addition of configuration interaction calculations on top of the CASSCF was necessary to obtain satisfactory results. The combination of one cerium 4^f electron and one ligand-based electron can lead to four possible electronic states (Figure 9).

The calculations supported an open-shell singlet ground state. The first excited state, an open-shell triplet, was found to be close in energy and only 40–75 cm⁻¹ higher in energy than the open-shell singlet ground state. In contrast, the 4^f closed-shell singlet is much higher in energy (> 400 cm⁻¹), and so is the 4^f closed-shell singlet.

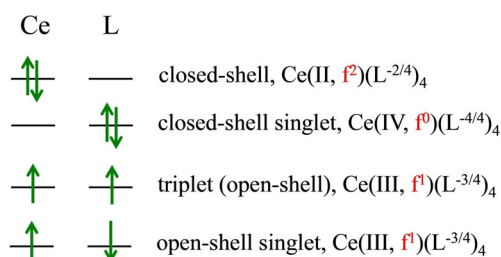


Figure 9. Different configurations considered. Adapted from Ref. [136].

Very recently, high-energy-resolution fluorescence detection X-ray absorption spectroscopy (HERFD-XAS) has been used to analyse a formal di-cerium(IV) phenolate complex and confirmed mixed valency with considerable 4^f character.^[138] In addition, the multiconfigurational ground state of formal Ce^{IV} complexes stabilised by imidophosphorane ligands or imidophosphorane-functionalised guanidinate ligands has been established through Ce L₃-edge XANES studies.^[139–141] Notably, the imidophosphorane Ce^{IV} complexes exhibited the lowest reported relative proportion of Ce^{III} L₃ character ($n_f=0.38(2)$). However, some limits to the dominant two-peak model in the analysis of the L₃-edge XANES spectra of tetravalent lanthanides were presented.^[140]

In 2019, access to the first molecular formal Tb^{IV} complexes has been described in independent reports by the groups of La Pierre and Mazzanti by using imidophosphorane and bulky siloxide ligands, respectively (Figure 10).^[19,20] The use of bulky Ph₃SiO ligands further allowed, in 2020, the synthesis of the first molecular Pr^{IV} complex.^[22] The reduction potential associated with the Pr^{IV}/Pr^{III} couple (+3.4 V) is very close to that of the Tb^{IV}/Tb^{III} couple (+3.3 V), which supports that similar ligand environments and procedures might be used to access both Tb^{IV} and Pr^{IV} complexes.^[21,22]

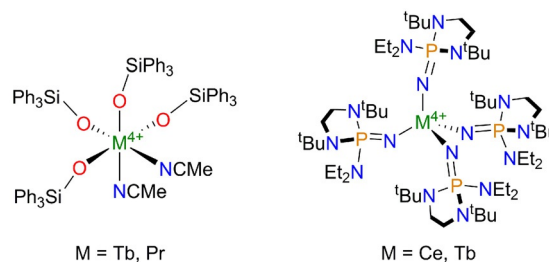


Figure 10. Recent ligand environments used for the stabilisation of formal tetravalent lanthanide compounds including Tb^{IV} and Pr^{IV} complexes.

The electronic structure of the imidophosphorane-stabilised Tb^{IV} complex was investigated by magnetic susceptibility, EPR and XANES studies.^[20] A multiconfigurational behaviour similar to that observed in TbO₂ was established by Tb L₃-edge XAS measurements. The characteristic double-peak structure was attributed to both Tb^{IV} and Tb^{III} configurations in the final state. The relative amount of the Tb^{III} L₃ character in the ground state has been evaluated to be 0.39(4), a value similar to that observed for TbO₂ (0.42(3)).^[111] These results indicate that ligand control of the multiconfigurational behaviour is of utmost importance to achieve stabilisation of formal Ln^{IV} complexes.

The multiconfigurational ground state established in these complexes shows that the mixed valency observed in formal Ln^{IV} compounds is not restricted to organometallic complexes but can be extended to other coordination compounds featuring electron-rich donor ligands.

2.7. [Cp*₂Yb(L)] adducts with L = N-heterocyclic redox-active ligands

The group of Andersen engaged in an in-depth study of the electronic structure and physical properties of ytterbocene adducts by using 2,2'-bipyridyl (bipy), 1,10-phenanthroline (phen) and other diazabutadiene (dad) ligands, which are known to be redox non-innocent or redox-active ligands (Figure 11).^[32,50,51,84,105,142–147] These compounds provide strong

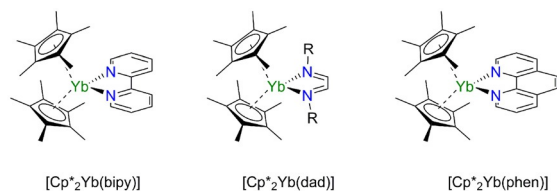


Figure 11. Structures of ytterbocene adducts with nitrogen-based redox-active ligands.

magnetic and spectroscopic evidence that both Yb^{II} f¹⁴ and Yb^{III} f¹³ configurations are represented in the ground state. In such complexes, depending on the ytterbocene substituents and on the nature of the ligand (bipy vs. phen), reduction of the redox-active ligand by the Yb^{II} centre may occur. The detailed analyses of the reasons allowing the transfer or not will be examined in section 3. In these complexes, the reduced nature of the bipyridyl ligand in [Cp*₂Yb(bipy)] can be qualitatively assessed by IR measurements where strong absorption bands in the regions 800–1000 cm⁻¹ and 1490–1575 cm⁻¹ are typical for a bipyridyl radical anion.^[84,142] In addition, analysis of the bond lengths within the bipyridyl ligand in the X-ray structures was indicative of the neutral or reduced character of the ligand and therefore of the ytterbium valence (for example, a variation in the C–C backbone distance of the bipy ligand from 1.49 (Yb^{II}) to 1.43 Å (Yb^{III}) was observed).^[50,84] The distance between the Yb and the centroid of the Cp* ligand was also suggested as an efficient probe of the ytterbium valence, with distances varying continuously from 2.74 (Yb^{II}) to 2.59 Å (Yb^{III}).^[51] Raman spectroscopy gave further evidence that the ligands in the [Cp*₂Yb(L)] (L = bipy, phen) adducts were reduced radical anions.^[85] Additionally, in the UV/Vis/near IR electronic absorption spectra of [Cp*₂Yb(L)] (L = bipy, phen), f–f transition bands typical of Yb^{III} compounds were detected but with some singularities.^[85] The intensities of the bands in the neutral complexes were 5–10 times greater than those in the corresponding oxidised cationic complexes, revealing unusually large oscillator strengths for f–f transitions. In the case of [Cp*₂Yb(phen)], the energies (ca. 11 000 cm⁻¹) and separations between adjacent f–f bands (ca. 510 and 780 cm⁻¹) were found significantly different from the values found in the cationic oxidised complex [Cp*₂Yb(phen)]⁺.^[85]

Magnetic studies on [Cp*₂Yb(L)] (L = bipy, phen) revealed that these complexes were not simple Yb^{II} f¹⁴ diamagnetic adducts. The magnetic moments at room temperature were lower than that expected for an Yb^{III} ion coordinated by a radi-

cal anionic ligand with non-interacting spins (4.5–5 μ_B). The low magnetic moment of the ground state can be explained by antiferromagnetic coupling between the Yb^{III} centre and the radical anion, and is consistent with the field dependence observed at low temperatures. The effective magnetic moment was also found to depend on the substituents on the cyclopentadienide rings (Cp*, Cp^{tt} (η⁵-1,3-tBu₂C₅H₃), Cp^{rr} (η⁵-1,3-(Me₃Si)₂C₅H₃)) and reflects the extent of electron transfer from the Yb^{II} centre to the N-heterocyclic ligand (see section 3).^[84] Although the 1/χ versus T plot of the phenanthroline adducts of Cp*₂Yb, Cp^{tt}₂Yb and (C₅Me₄H)₂Yb featured as expected a linear dependence, a nonlinear shape was observed for [Cp*₂Yb(bipy)] and [(C₅Me₄H)₂Yb(bipy)] with a maximum χ value at 380 K. Similarly, analysis of the ¹H NMR spectra of [Cp*₂Yb(bipy)] at variable temperatures revealed a nonlinear plot for δ versus 1/T, which cannot be explained by a Curie–Weiss behaviour.^[84] More generally, variable-temperature analysis of the ¹H NMR chemical shifts of ytterbocene adducts constitutes a useful tool to probe the magnetic behaviour, especially to reveal intermediate valence.^[143,144,146] Further investigation of the magnetic properties was carried out by using the sealed quartz tube technology, allowing a more precise determination of the magnetic moment for highly air-sensitive and weakly paramagnetic compounds, which feature low but non-zero values of μ.^[142] This is especially the case for [Cp^{tt}₂Yb(bipy)] and [Cp^{rr}₂Yb(bipy)], which were found to be weakly paramagnetic. Their 1/χ versus T plots were significantly curved but did not exhibit the unusual behaviour evidenced in [Cp*₂Yb(bipy)] and [(C₅Me₄H)₂Yb(bipy)]. To account for the unusual magnetic behaviour observed in bipyridine, phenanthroline and in a related 4'-cyanoterpyridyl adduct of ytterbocene, a thermally induced valence tautomeric equilibrium between paramagnetic 4f¹³–π*¹ and diamagnetic 4f¹⁴–π*⁰ forms was first suggested.^[84,85,148] However, the lack of temperature dependence of the ytterbium valence observed in XANES studies^[50,105,145] and variable-temperature electronic absorption spectra^[149] were not consistent with valence tautomerism. Moreover, the higher contribution of the Yb^{II} 4f¹⁴–π*⁰ configuration at low temperature was not consistent either with genuine redox-isomerism in a lanthanide complex. Indeed, valence tautomerism being an entropy-driven process, the isomeric form with the shorter metal–ligand bond lengths, that is, involving the more oxidised Yb^{III} ion, should be stabilised at lower temperatures.^[150,151]

For many ytterbocene adducts, temperature-independent paramagnetism (TIP) was observed at low temperatures, which can be interpreted as a van Vleck interaction between the ground-state singlet and the triplet configuration at some higher energy.^[50] The magnetic behaviour can be explained by a multiconfigurational singlet ground state, with contributions of both Yb^{II} f¹⁴ and Yb^{III} f¹³ configurations, which is lower in energy than the triplet configuration. When the temperature thermally allows the population of the triplet configuration, the susceptibility initially increases (out of the TIP regime) and then decreases, as in a conventional Curie–Weiss paramagnet.^[50]

In the case of methyl-substituted bipyridine and phenanthroline adducts of ytterbocene, unusual magnetic susceptibility data were observed and supported a temperature-dependent variation of the Yb valence.^[51,145,147] In several cases, the presence of inflection points was observed in the plots of χT versus T , which was rationalised by a multiconfigurational open-shell singlet ground state with low-lying excited states.^[51,146,152] Especially, different open-shell singlets were found below the triplet state and their thermal population with increasing temperatures accounts for the unusual temperature dependence of the magnetic data (see below). Ab initio calculations were first performed by using the model $[\text{Cp}_2\text{Yb}(\text{bipy})]$ compound,^[50] and further improved by using Cp^* (instead of Cp) fragments.^[51] Such calculations typically involve a first DFT geometry optimisation of the molecule using small core Relativistic Effective Core Potentials (RECP)^[120,121,123,153] followed by CASSCF calculations. After testing active spaces of different sizes and careful comparison of the results, the smallest active space giving the same qualitative results was used for the complete calculations.^[154] To obtain a better adequation between the calculations and the experimental results, a larger active space that included additional π^* configurations for the substituted bipyridine ligand was used in the computational model and a perturbative PT2 correction was added.^[51] The calculations revealed that the ground states and first excited states were dependent on the number and position of the methyl substituents.^[51,145,147] In addition, a correlation between the relative populations of the f^{13} and f^{14} configurations and the redox properties of the two fragments (ytterbocene and redox-active ligand) was established.^[145]

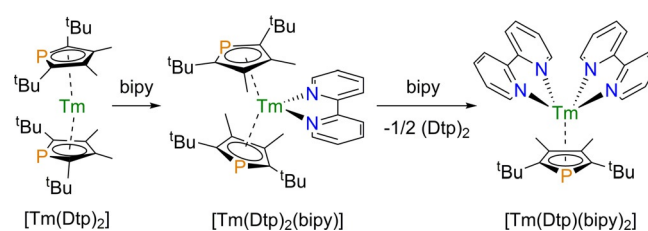
To support the magnetism studies, Yb L_3 -edge XANES data of $[\text{Cp}^*_2\text{Yb}(\text{bipy})]$ were recorded at different temperatures. The f-hole occupancy (n_f), which is directly linked to the ytterbium valence ($v=2+n_f$), was estimated to be 0.80 ± 0.03 for $[\text{Cp}^*_2\text{Yb}(\text{bipy})]$ without any change from 10 K up to decomposition at above approximately 400 K.^[105] Similar results were obtained for a series of 4,4'-disubstituted bipyridine and 1,4-diazabutadiene (dad) adducts of ytterbocene, which were found to feature between 83 and 95% of trivalent character with no significant change of the lanthanide valence with temperature (in the range 20–300 K).^[50] In methyl-substituted bipyridine adducts of ytterbocene, depending on the number and position of the methyl substituents, Yb L_3 -edge XANES data revealed different contributions of the Yb^{II} and Yb^{III} forms with temperature and therefore temperature-dependent variation of the Yb valence.^[51,145,147]

In addition, the coordination of unsubstituted imino-pyridine ligands to Cp^*_2Yb resulted in an electronic transfer reaction and formation of an Yb^{III} complex featuring a radical-anionic ligand.^[155] Variable-temperature magnetic measurements revealed a maximum at 170 K in the χ_M versus T data, consistent with a multiconfigurational ground state for the Yb ion. Ab initio calculations (CASSCF) using the same methodology as above, supported an open-shell singlet ground state constituted of 78% Yb^{III} and 22% Yb^{II} .

CASSCF and CASPT2 calculations were also carried out on the 1,4-diazabutadiene (dad) $[\text{Cp}^*_2\text{Yb}(\text{dad})]$ and $[\text{Ind}_2\text{Yb}(\text{dad})]$ ($\text{Ind} = \eta^5\text{-C}_9\text{H}_7$) complexes.^[156] Owing to the near degeneracy of the low-lying electronic states, DFT methods were again not appropriate to determine the correct electronic ground state of the system and explain its magnetic properties. Both ligands on the ytterbium centre, Cp^* and indenyl on the one hand, bipy and DAB on the other hand, were found to have an effect on the electronic ground-state configuration. Only one of the possible ligand combinations, corresponding to the diamagnetic $[\text{Ind}_2\text{Yb}(\text{bipy})]$ complex, could be properly studied by using a standard single-configuration DFT approach. Compared with ab initio calculations, DFT calculations are less computationally demanding and can be applied to the real molecules. In contrast, ab initio calculations are typically performed on reduced model systems. The latter should, however, be realistic enough to reproduce the electronic complexity and specificities of the experimental systems.

2.8. Other lanthanide complexes with redox-active ligands

Multiconfigurational ground states were also invoked to rationalise the unusual magnetic properties of bipyridine and bisphosphinine (phosphorus analogues of bipyridine) adducts of bis(phospholyl) thulium(II) ($[\text{Tm}(\text{Dtp})_2]$, see Scheme 3) but the precise electronic structures of the complexes have remained elusive to date.^[157]



Scheme 3. Synthesis and reactivity of a bipyridine adduct of $[\text{Tm}(\text{Dtp})_2]$.^[157]

Recently, the electronic structures of lanthanide tetrakisbipyridine complexes were investigated.^[158] Both magnetic susceptibility measurements and L_3 -edge XANES data on the Ce and Yb species were consistent with the metals being trivalent. CASSCF calculations were performed on the closed-shell La^{III} and Lu^{III} (f^0 and f^{14} configuration, respectively) complexes, as well as on the Ce^{III} and Yb^{III} derivatives featuring one f-electron (f^1) or one f-hole (f^{13}), respectively. The different multiconfigurational nature of the corresponding ground states helped understand the slight differences observed in their physical properties such as subtle bond length variations and magnetic susceptibility dependencies with temperature. For such systems, multireference calculations,^[57,58] as opposed to single reference DFT calculations, are often necessary to properly reproduce some of the physical properties such as temperature dependency of the magnetic susceptibility.

2.9. Concluding remarks on spectroscopic singularities

The systems presented above can be considered molecules in which the oxidation number is ambiguous and they are representatives of intermediate valence compounds using the term as defined by the physics community. The contribution of the ligand and metal charge transfer configuration will allow the formation of a state, in which the covalency, that is, the electronic delocalisation extent, is substantial. Clearly, in Yb, Eu, Tm and Ce compounds, the redox potential is adapted for these charge transfers with the ligand. It would mean that the energy match or mismatch between ligand and metal orbitals is at the origin of the situation the phenomenon; at least as much as the symmetry consideration for spatial overlap.

3. Energy and Symmetry Considerations

All these spectroscopic singularities, reinforced by adapted theoretical computations, clearly established that coordination compounds (or organometallics) of lanthanides can develop intermediate-valent states, that is, multiconfigurational energy states with configurations featuring different oxidation states. In these compounds, the relative ratio between their configurations varies and can be quantified from adapted experimental measurements and confirmed by adapted theoretical computations. An important point going forward is the rationalisation of this ratio from simple symmetric and energetic considerations.

The covalency represents the extent of the electronic delocalisation over both the metallic and ligand sites, as defined by Neidig and co-authors [Equation (2)].^[34] In this description, to allow a non-zero mixing coefficient, that is, covalency, two parameters are at play: the ligand and metal orbital overlap, and the energy difference between both fragments. In lanthanide compounds, little overlap is expected between these orbitals as f-orbitals are core orbitals. Nevertheless, according to Equation (2), the covalency can also be maximised when the energy gap is minimised. In this situation, the electronic density is statistically delocalised over both the ligand and metal radical, leading to an intermediate-valent charge at the lanthanide centre.

$$\sigma = \frac{\varphi_M + \lambda\varphi_L}{\sqrt{1 + 2\lambda S_{ML} + \lambda^2}} \quad \lambda = \frac{H_{ML}}{E_M^0 - E_L^0} \quad (2)$$

where σ is the mixing metal and ligand orbital from perturbation theory of the ionic limit, φ_M is the metal orbital and φ_L the ligand orbital, both characterised by the metal and ligand energies, E_M^0 and E_L^0 . S_{ML} is the orbital overlap, λ the mixing coefficient and H_{ML} the off-diagonal matrix element of the Hamiltonian. Note that in the Hückel theory, H_{ML} is proportional to S_{ML} .

For example, if [U(Cot)₂] and [Ce(Cot)₂] are compared,^[106] the former has greater metal–ligand overlap, whereas the latter has better metal–ligand energy matching, which results in so-called “degeneracy-driven covalency”,^[34] and participates in the bonding while simultaneously appearing localised.

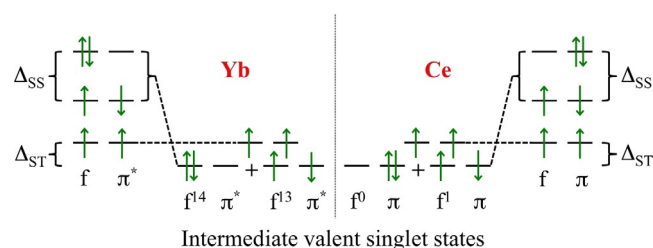


Figure 12. Qualitative energy level diagram showing the origin of the intermediate valence states for ytterbium and cerium complexes.

Overall, in Ce and Yb complexes, the description is simpler. They are empty—or full shell—in one configuration and singly occupied—or having only one hole—in the other. The energy diagram of both cases is shown in Figure 12.^[50] The mixing of the singlet configurations results in a multiconfigurational state of lower energy, in which the two configurations have different valency, leading to intermediate-valent states. It is clear from this energy scheme that the energy difference between the open-shell and closed-shell singlets, Δ_{SS} , and the energy gap singlet-triplet Δ_{ST} are going to govern the overall electronic structure.

As discussed above, a series of complexes with substituted bipyridine and diazabutadiene ligands with the Cp*₂Yb fragments has been synthesised in several articles from the Andersen group.^[51,145] The energy of the ligand fragment and that of the metal fragment, E_M and E_L , which is intimately related to Δ_{SS} , can be extrapolated from their respective redox potentials.^[50,145] As written in the previous paragraph, L₃-edge XANES data indicated an n_f value of 0.83 for [Cp*₂Yb(bipy)], that is, an intermediate-valent ground state composed of 83% Yb^{III} and 17% Yb^{II}. This ratio can evolve depending upon the substituents added to the bipy, which change the ligand redox potential. In other words, when substituents decrease the redox potential, the n_f value becomes lower and the valency closer to Yb^{II}. Likewise, when substituents increase the redox potential, the n_f gets closer to 1 and the net valency approaches that of Yb^{III}. This effect can be easily verified by synthesising the 3,3'-Me₂bipy adduct of Cp*₂Yb, which has a n_f value of 0.17(2) for a reduction potential of the ligand below −2.8 V (Figure 13).

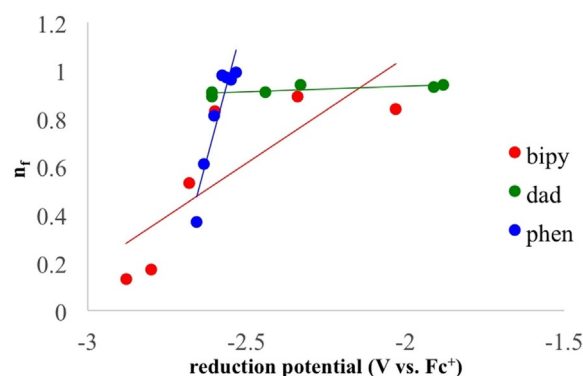


Figure 13. Plot of the redox potentials of the (substituted) bipy, phen and dad ligands taken from the literature^[50,145,159,160] versus the measured n_f for each series. Linear fitting is only to guide the eye.

This relatively low reduction potential is due to the steric hindrance of the two methyl groups, which are close to each other, inducing a NCCN torsion angle that lowers the reduction potential. As an additional note, when the reduction potential of the metallic fragment is increased, for example, when the Cp* ligand is replaced by the Cp ligand, the n_f also decreases; the n_f of [Cp*₂Yb(bipy)] is 0.83(2) whereas that of [Cp₂Yb(bipy)] is 0.30(1).

The problem became more complex after another series of substituted bipyridine ligands exhibited multiple intermediate valence singlet states below the triplet state. This situation is possible when several low-lying π^* orbitals of the ligand are close enough to accommodate spin density from the Cp*₂Yb fragment; each orbital then has a configuration with a given ratio (n_f). Figure 14 represents a typical situation. The different natures of the multiple intermediate-valent singlet states were identified thanks to the L₃-edge XANES data combined with the temperature-dependent magnetic data. As a result of the different ratio in each configuration, the overall n_f and thus the intermediate valency becomes temperature dependent. The corresponding thermodynamic parameters can be extracted by fitting the temperature-dependent n_f by using a Boltzmann distribution; these values can be then incorporated in the analysis of the magnetic data.

In the case of 4,5-diazafluorene, the magnetic data indicated three singlet states below the triplet, coming from three low-lying empty π^* orbitals (Figure 14).^[146]

However, if the energetic consideration described above helped to estimate the n_f ratio within one series of ligands, a quick look at Figure 13 also indicates that the correlation between the redox potential and the n_f cannot be generalised and remained true only within each ligand series, the bipy, the phen and the dad series. Additionally, this correlation remained also problematic in the case of the higher energy singlet states (below the triplet) of the substituted bipy ligands. This situation thus tended to indicate that the energy is not the single factor controlling the intermediate valency: the second impor-

tant parameter is the symmetry of the π orbital that accepts the electron. The correlation between redox potential and n_f value is valid only for orbitals of similar symmetry.

In this matter, the study of the phenanthroline series was of great importance as the ligand is known to possess two empty π orbitals of similar energy that have two very different symmetries.^[161] In C_{2v} symmetry, these two orbitals have b₁ and a₂ symmetry (Figure 15); b₁ is similar to the low-lying orbital of bipyridine and has much density located on the nitrogen atoms, which coordinate to the lanthanide metal centre; a₂, however, has very little density on the nitrogen atoms and a node at the 3,8-position of the phenanthroline. A molecular orbital diagram of the f-shell orbitals indicated that the singly occupied f-orbital possesses b₁ symmetry in C_{2v}.^[32,147]

Thus, as opposed to the bipy adduct, the phen adduct was analysed as a triplet, meaning that the symmetry orbital requirements must also be validated to stabilise the intermediate-valent singlet state. Interestingly, depending upon the substituents and their positions, the ground state can be different (triplet or intermediate valent). This means that the relative energy between the different symmetry orbitals can be modulated,^[161] which then leads to the modulation of the ground state as shown by the temperature-dependent magnetic data and L₃-edge XANES.^[32,145–147] An important example is the 3,8-phenanthroline adduct of ytterbocene. Indeed, as the a₂ orbital possesses a node at the 3,8-position, when a methyl replaces the hydrogen at these positions, the energy of the a₂ is not modified whereas that of the b₁ is slightly increased; the ground state is then similar to that of the phen analogue, which is triplet (Figure 16). Accordingly, donating substituents at the 5,6-positions increase the energy of the a₂ and slightly increase that of the b₁, leading to a situation in which both orbitals have similar energies; the singlet and triplet states have similar energies. Now, when substituents are at the 4,7-positions, the energies of both orbitals are increased but one should note that the coordination of the ytterbium fragment lowers the energy of the b₁ as much density is located in the nitrogen atoms. Thus, the b₁ becomes lower in energy and the ground state is the intermediate-valent singlet (Figure 16).

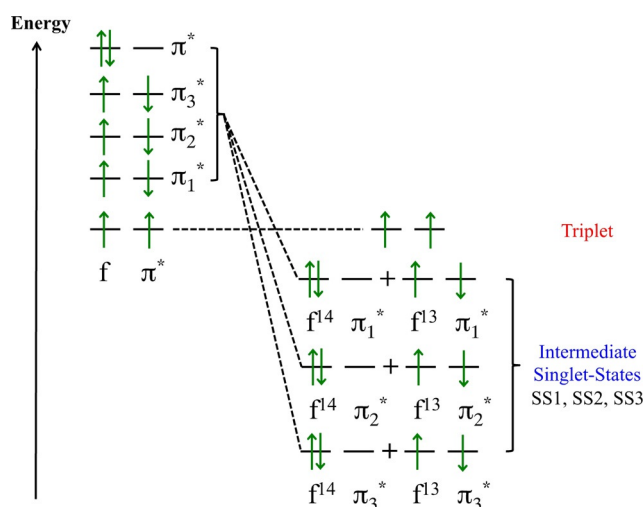


Figure 14. Energy scale with multiple π^* orbitals accepting electronic density and forming multiple intermediate-valent singlet states below the triplet.

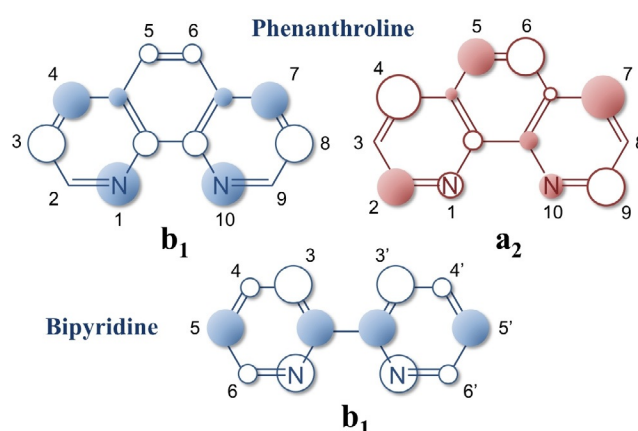


Figure 15. Representation of the π^* orbitals for bipy and phen and numbering positions.

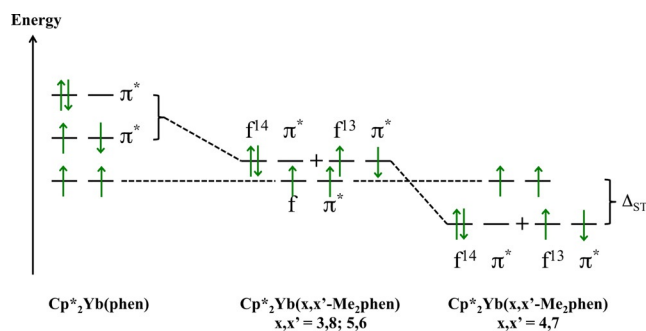
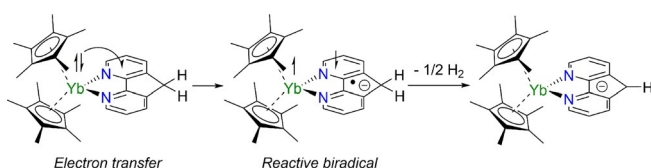


Figure 16. Qualitative MO diagrams showing the influence of the nitrogenated ligand on the electronic structure of the resulting complex.^[147]

As it has been noted early in the literature, intermediate valence state compounds are interesting molecular Kondo systems.^[47] This phenomenon can occur in nanometre-sized metallic particles and is explained by the presence of paramagnetic impurities, which break the continuous conduction band and creates localised conduction states.^[64,65] In the case of the Ce and Yb compounds discussed above, the f-moment is cancelled by coupling with extended conjugated π systems such as bipyridine, phenanthroline, but also Cot and tropolonate among others. Additionally, the formation of these intermediate-valent states also demonstrated that the exchange coupling of a radical spin with f-electrons can be rather large, compared with what is usually known in magnetic coupling involving f-elements. Using a model that combined the ligand-to-metal charge transfer energy (Hubbard model), it was possible to determine an exchange coupling value of -920 cm^{-1} for $[\text{Cp}^*_2\text{Yb}(\text{bipy})]$.^[162] This very large value also explains why the use of extended π systems is particularly relevant for the design of compounds with high magnetic coupling between lanthanides. The presence of a π -radical between lanthanide metal centres increases greatly the coupling between them and led notably to performing single molecules magnets.^[163–166]

4. Chemical Ramifications

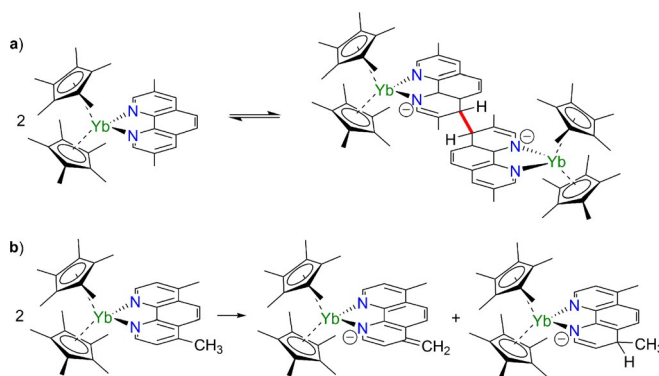
The symmetry of the orbitals became a crucial consideration when talking about reactivity as was demonstrated when the bipy was switched for other di-nitrogenated ligands such as diazafluorene and phenanthroline.^[32,146,147] The $[\text{Cp}^*_2\text{Yb}(4,5\text{-diazfluorene})]$ complex was shown by Nocton et al. to slowly release H_2 , leading to the corresponding $[\text{Cp}^*_2\text{Yb}(4,5\text{-diazfluorenyl})]$ complex (Scheme 4).^[146] Experimental and computational studies indicated that the electronic structure of the com-



Scheme 4. Elimination of H_2 from the 4,5-diazfluorene ligand triggered by the intermediate-valent behaviour.^[146]

pound was similar to that of bipyridine adducts of Cp^*_2Yb with an intermediate-valent ytterbium centre and two open-shell singlet states lying below the triplet state. Analysis of the π^* orbitals of the ligand revealed that the LUMO + 1 orbital of the fluorene was of b_1 symmetry in the C_{2v} space group and featured non-negligible spin density on the C9 carbon atom. The presence of unpaired spin density at this position helped to rationalise the observed reactivity. It is thought that the electronic structure of $[\text{Cp}^*_2\text{Yb}(4,5\text{-diazfluorene})]$, and the formation of a reactive biradical, is responsible for the C–H activation reaction.^[146] Importantly, the configuration interaction allowed the LUMO + 1 to be substantially populated at room temperature (see Figure 14, energy of SS1, SS2, SS3), the one orbital responsible for the observed reactivity. In contrast, the biradical adducts formed in the case of bipyridine adducts of ytterbocene was more stable and not involved in further chemical evolutions.

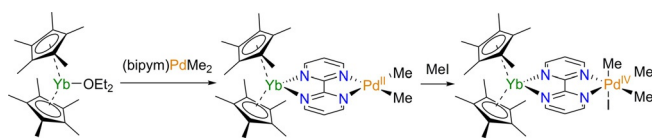
The influence of orbital symmetries on the reactivity was further evidenced in the $[\text{Cp}^*_2\text{Yb}(\text{phen})]$ complex and its methylated analogues.^[32,147] Experimental and computational results revealed a triplet ground state with a trivalent ytterbium centre, which contrasts with the open-shell singlet ground state of the bipyridine adducts. Such a different electronic structure has a direct influence on the reactivity of the complexes. Indeed, the $[\text{Cp}^*_2\text{Yb}(\text{phen})]$ complex, as well as the (3,8)- and (5,6)-di-methylated analogues, dimerised in solution with formation of a reversible C–C bond between the two phenanthroline moieties at the 4,4'-positions (Scheme 5). This unusual reactivity originates in the energy and symmetry of the ligand empty orbitals. In the phenanthroline complex, two π^* orbitals of different symmetry (b_1 and a_2 for the LUMO and LUMO + 1, respectively) are accessible but their respective interaction with either the half-filled 4f orbitals of b_1 symmetry or the empty 5d orbitals of a_2 symmetry results in different cases. As discussed above, on the one hand, if the b_1 orbital is lower in energy than the a_2 orbital, an open-shell singlet ground state is favoured, as is the case in the bipyridine adducts of Cp^*_2Yb . On the other hand, if the ligand a_2 and b_1 orbitals are close in energy, as is the case in the phenanthroline adducts, the final a_2 MO ends up lower in energy, resulting in



Scheme 5. Two different reactivities observed for two different phenanthroline derivatives (a) C4–C4' coupling, (b) C4-position-mediated intermolecular HAT.^[32,147]

stabilisation of the triplet ground state (Figure 16). As this result is based on the energy of the phenanthroline ligand orbitals, it can be tuned by the presence of methyl substituents affecting the b_1 - a_2 gap. The population of the a_2 orbital results in an increased spin density in the π system especially at the C4 and C7 positions. The radical character at these positions is responsible for the formation of a reversible C–C bond between the two phenanthroline units (Scheme 5).^[32] Nonetheless, when the phenanthroline is substituted at the 4,7-positions with methyl groups, a different configuration is observed, with a multiconfigurational open-shell singlet ground state.^[147] The altered electronic structure, similar to that observed in the bipyridine adducts, results in a different reactivity. In $[\text{Cp}^*_2\text{Yb}(4,7\text{-Me}_2\text{phen})]$, accumulation of electronic density at the C4 and C7 positions leads to an intermolecular hydrogen atom transfer (HAT) reaction between two complexes (Scheme 5), reminiscent of the H_2 elimination reactivity observed in the case of the diazafluorene complex.^[146,147]

Taking advantage of the particular and tuneable electronic structures of $[\text{Cp}^*_2\text{Yb}(\text{L})]$ systems, the influence of the ligand was further explored to modulate the chemical reactivity. The possibility of impacting the reactivity of another metal centre was explored through the formation of heterobimetallic complexes using bridging 2,2'-bipyrimidine (bipym) and 4,5,9,10-tetraazaphenanthrene (taphen) ligands instead of bipyridine and phenanthroline ligands. In 2017, the group of Nocton reported the syntheses and electronic structures of the Yb/Pd heterobimetallic complexes $[\text{Cp}^*_2\text{Yb}(\text{L})\text{PdMe}_2]$ ($\text{L} = \text{bipym}$ or taphen; Scheme 6).^[152] Depending on the nature of the ligand, different electronic structures were observed owing to different symmetries for the corresponding LUMOs. In the bipym system, similarly to bipyridine adducts of ytterbocene, the ground state is a multiconfigurational open-shell singlet with a low-lying triplet state populated at room temperature. In contrast, the taphen complex features a triplet ground state, in analogy with the ground-state structure of the phenanthroline adduct of Cp^*_2Yb . The influence of the different electronic structures on the reactivity was exemplified in the reactivity of the complexes towards MeI. In both cases, the addition of MeI triggered an oxidative addition step, resulting in the formation of a Pd^{IV} complex. Although the resulting Pd^{IV} complex rapidly evolved through a reductive elimination process in the taphen system, it presented a much higher stability in the case of the bipym ligand, allowing isolation and characterisation. The increased stability of the $[\text{Cp}^*_2\text{Yb}(\text{bipym})\text{PdMe}_2]$ complex is mainly due to the spin density mostly held by the N atoms in the b_1 orbital, which support the Pd centre. In the taphen analogue instead, the a_2 orbital is populated and features smaller coefficients on the N atoms. As a result, a lower spin density is



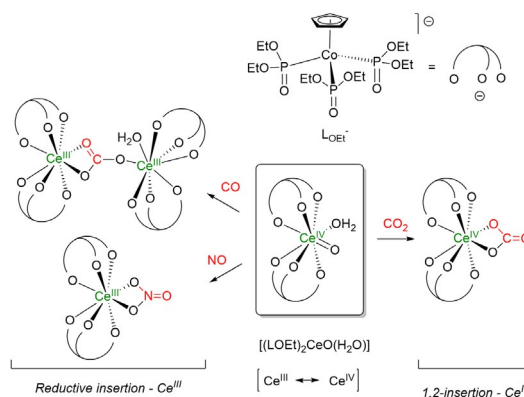
Scheme 6. Heterobimetallic Yb–Pd association leading to the stabilisation of a Pd^{IV} oxidation state.^[152]

present next to the Pd centre, which decreases the stability of the high oxidation state Pd^{IV} complex and triggers a fast reductive elimination step as expected for such Pd^{IV} species.^[152]

Another chemical ramification of the electronic structure of heterobimetallic complexes was reported with the same $\text{Cp}^*_2\text{Yb}(\text{bipym})$ backbone using a NiMe_2 fragment instead of PdMe_2 .^[167] Both the monometallic $[(\text{bipym})\text{NiMe}_2]$ and the heterobimetallic $[\text{Cp}^*_2\text{Yb}(\text{bipym})\text{NiMe}_2]$ complexes were found to react with CO, resulting in CO insertion reactions in the Ni–C bonds. Kinetic studies revealed that the intermediate-valent lanthanide-bipym fragment led to an increased stabilisation of the expected acyl intermediate through a process similar to that allowing the stabilisation of the Pd^{IV} complex discussed above.^[167] This result offers a new strategy to stabilise and study reactive metal intermediates for which isolation has remained elusive to date.

The influence of the multiconfigurational character of lanthanide complexes on the reactivity was further exemplified in the case of Ce^{IV} oxo complexes supported by the bulky Kläui oxygen tripod ligand $[\text{CoCp}\{\text{P}(\text{O})(\text{OEt})_2\}_3]^-$ (LOEt^- , Scheme 7).^[168,169]

The multiconfigurational character of the $[(\text{LOEt})_2\text{CeO}(\text{H}_2\text{O})]$ complex was established by CASSCF calculations together with magnetic susceptibility measurements. The combined experimental and theoretical results revealed a multiconfigurational ground state composed of 74% of Ce^{IV} and 26% of Ce^{III} . The reactivity of the oxocerium(IV) complexes was evaluated towards small molecules such as CO, CO_2 , SO_2 and NO. Depending on the substrate, two different types of reactivity for the $\text{Ce}=\text{O}$ moiety were observed (Scheme 7). Although a classical 1,2-insertion reactivity was observed with CO_2 , which corresponds to the typical reactivity of Ce^{IV} f^0 complexes, the reaction with CO, SO_2 and NO resulted in an unusual reductive insertion reactivity. As a result, (bi)carbonate, hydrogensulfate and nitrate Ce^{III} complexes were isolated, respectively. Such a reductive insertion reactivity is thought to arise from the multiconfigurational nature of the ground state, the $\text{Ce}=\text{O}$ moiety featuring both some Ce^{IV} oxo and Ce^{III} oxyl character. The Ce^{III} oxyl character results in a radical-like reactivity by forming a singlet metal–ligand biradical similar to the situation in cerocene.^[169]



Scheme 7. Schematic representation of the reactivity of the oxocerium complex $[(\text{LOEt})_2\text{CeO}(\text{H}_2\text{O})]$.^[169]

6. Concluding Remarks

The minireview gathers the spectroscopic singularities that have been reported for lanthanide compounds. In these compounds, the net valency remains ambiguous because of possible redox events with the ligand, whether charge density is transferred from the ligand to the metal or from the metal to the ligand. In addition to physical chemistry reports containing XANES, PES and/or magnetic analysis, adapted theoretical analyses of these peculiar compounds have allowed the rationalisation of their original electronic nature: they are intermediate valent; the wavefunction of the ground and excited state is defined by multiple configurations, in which the valency is of different nature. These observations can be rationalised first from energetic considerations, as the result of the energy difference between both metallic and ligand fragments, and second from the symmetry of both fragments, which needs to be adapted to allow stabilisation of the energy with formation of an intermediate-valent energy state. This typical situation is predominant in lanthanide compounds, in which the spatial orbital overlap is small, whereas in transition metal ions or 5f complexes, the nephelauxetic effect allows the formation of molecular orbitals with delocalised electron density over both the metallic and ligand centres (so-called covalency). Both situations are, however, similar from the perspective of the Pauling electroneutrality principle. As well-established for transition metals and for 5f compounds, the strong electron correlation between a d- and/or f-parentage electron and the σ - and π -electron is then likely to influence the physical properties (relaxation, anisotropy, conductivity) but also the reactivity of these electrons: this review sheds light on several examples of this nature.

Acknowledgments

This work is part of a project that has received funding from the *European Research Council (ERC)* under *European Union's Horizon 2020 research and innovation program* under grant agreement No 716314. CNRS and Ecole polytechnique are thanked for funding.

Conflict of interest

The authors declare no conflict of interest.

Keywords: intermediate valence · lanthanides · organometallics · spectroscopy · theoretical computations

- [1] J.-C. G. Bünzli, C. Piguet, *Chem. Soc. Rev.* **2005**, *34*, 1048–1077.
- [2] S. Cotton in *Lanthanide and Actinide Chemistry*, Wiley, Chichester, **2006**, pp. 61–87.
- [3] E. G. Moore, A. P. S. Samuel, K. N. Raymond, *Acc. Chem. Res.* **2009**, *42*, 542–552.
- [4] D. N. Woodruff, R. E. P. Winpenny, R. A. Layfield, *Chem. Rev.* **2013**, *113*, 5110–5148.
- [5] J.-L. Liu, Y.-C. Chen, M.-L. Tong, *Chem. Soc. Rev.* **2018**, *47*, 2431–2453.

- [6] B. M. Day, F.-S. Guo, R. A. Layfield, *Acc. Chem. Res.* **2018**, *51*, 1880–1889.
- [7] R. Pöttgen, T. Jüstel, C. A. Strassert, *Rare Earth Chemistry*, De Gruyter, Berlin, **2020**, pp. 1–654.
- [8] J.-C. G. Bünzli in *Kirk-Othmer Encyclopedia of Chemical Technology*, **2013**, pp. 1–43.
- [9] D. A. Atwood, *The Rare Earth Elements: Fundamentals and Applications*, Wiley, Chichester, **2013**, pp. 1–654.
- [10] P. Pyykko, *Chem. Rev.* **1988**, *88*, 563–594.
- [11] M. N. Bochkarov, *Coord. Chem. Rev.* **2004**, *248*, 835–851.
- [12] P. B. Hitchcock, M. F. Lappert, L. Maron, A. V. Protchenko, *Angew. Chem. Int. Ed.* **2008**, *47*, 1488–1491; *Angew. Chem.* **2008**, *120*, 1510–1513.
- [13] F. Nief, *Dalton Trans.* **2010**, *39*, 6589–6598.
- [14] M. R. MacDonald, J. E. Bates, M. E. Fieser, J. W. Ziller, F. Furche, W. J. Evans, *J. Am. Chem. Soc.* **2012**, *134*, 8420–8423.
- [15] M. R. MacDonald, J. E. Bates, J. W. Ziller, F. Furche, W. J. Evans, *J. Am. Chem. Soc.* **2013**, *135*, 9857–9868.
- [16] M. E. Fieser, M. R. MacDonald, B. T. Krull, J. E. Bates, J. W. Ziller, F. Furche, W. J. Evans, *J. Am. Chem. Soc.* **2015**, *137*, 369–382.
- [17] C. M. Kotyk, M. E. Fieser, C. T. Palumbo, J. W. Ziller, L. E. Darago, J. R. Long, F. Furche, W. J. Evans, *Chem. Sci.* **2015**, *6*, 7267–7273.
- [18] W. J. Evans, *Organometallics* **2016**, *35*, 3088–3100.
- [19] C. T. Palumbo, I. Zivkovic, R. Scopelliti, M. Mazzanti, *J. Am. Chem. Soc.* **2019**, *141*, 9827–9831.
- [20] N. T. Rice, I. A. Popov, D. R. Russo, J. Bacsa, E. R. Batista, P. Yang, J. Telsler, H. S. La Pierre, *J. Am. Chem. Soc.* **2019**, *141*, 13222–13233.
- [21] A. R. Willauer, C. T. Palumbo, R. Scopelliti, I. Zivkovic, I. Douair, L. Maron, M. Mazzanti, *Angew. Chem. Int. Ed.* **2020**, *59*, 3549–3553; *Angew. Chem.* **2020**, *132*, 3577–3581.
- [22] A. R. Willauer, C. T. Palumbo, F. Fadaei-Tirani, I. Zivkovic, I. Douair, L. Maron, M. Mazzanti, *J. Am. Chem. Soc.* **2020**, *142*, 5538–5542.
- [23] T. P. Gomba, A. Ramanathan, N. T. Rice, H. S. La Pierre, *Dalton Trans.* **2020**, *49*, 15945–15987.
- [24] M. E. Fieser, M. G. Ferrier, J. Su, E. Batista, S. K. Cary, J. W. Engle, W. J. Evans, J. S. Lezama Pacheco, S. A. Kozimor, A. C. Olson, A. J. Ryan, B. W. Stein, G. L. Wagner, D. H. Woen, T. Vitova, P. Yang, *Chem. Sci.* **2017**, *8*, 6076–6091.
- [25] N. Li, W.-X. Zhang, *Chin. J. Chem.* **2020**, *38*, 1449–1450.
- [26] E. Prasad, B. W. Knettle, R. A. Flowers, *J. Am. Chem. Soc.* **2004**, *126*, 6891–6894.
- [27] K. A. Choquette, D. V. Sadasivam, R. A. Flowers, *J. Am. Chem. Soc.* **2010**, *132*, 17396–17398.
- [28] X. Zhao, L. Perrin, D. J. Procter, L. Maron, *Dalton Trans.* **2016**, *45*, 3706–3710.
- [29] W. J. Evans, J. W. Grate, L. A. Hughes, H. Zhang, J. L. Atwood, *J. Am. Chem. Soc.* **1985**, *107*, 3728–3730.
- [30] W. J. Evans, T. A. Ulibarri, J. W. Ziller, *J. Am. Chem. Soc.* **1988**, *110*, 6877–6879.
- [31] S. Labouille, F. Nief, X.-F. Le Goff, L. Maron, D. R. Kindra, H. L. Houghton, J. W. Ziller, W. J. Evans, *Organometallics* **2012**, *31*, 5196–5203.
- [32] G. Nocton, W. W. Lukens, C. H. Booth, S. S. Rozenel, S. A. Medling, L. Maron, R. A. Andersen, *J. Am. Chem. Soc.* **2014**, *136*, 8626–8641.
- [33] G. Nocton, L. Ricard, *Chem. Commun.* **2015**, *51*, 3578–3581.
- [34] M. L. Neidig, D. L. Clark, R. L. Martin, *Coord. Chem. Rev.* **2013**, *257*, 394–406.
- [35] D. G. Karraker, *J. Chem. Educ.* **1970**, *47*, 424.
- [36] K. N. Raymond, C. W. Eigenbrot, *Acc. Chem. Res.* **1980**, *13*, 276–283.
- [37] S. Cotton in *Lanthanide and Actinide Chemistry*, Wiley & Sons, Chichester, **2006**, pp. 35–60.
- [38] N. C. Tomson, M. R. Crimmin, T. Petrenko, L. E. Rosebrugh, S. Sproules, W. C. Boyd, R. G. Bergman, S. DeBeer, F. D. Toste, K. Wieghardt, *J. Am. Chem. Soc.* **2011**, *133*, 18785–18801.
- [39] K. Ray, T. Weyhermüller, F. Neese, K. Wieghardt, *Inorg. Chem.* **2005**, *44*, 5345–5360.
- [40] K. Ray, T. Petrenko, K. Wieghardt, F. Neese, *Dalton Trans.* **2007**, 1552–1566.
- [41] C. C. Scarborough, S. Sproules, T. Weyhermüller, S. DeBeer, K. Wieghardt, *Inorg. Chem.* **2011**, *50*, 12446–12462.
- [42] C. C. Scarborough, K. Wieghardt, *Inorg. Chem.* **2011**, *50*, 9773–9793.
- [43] N. C. Tomson, K. D. Williams, X. Dai, S. Sproules, S. DeBeer, T. H. Warren, K. Wieghardt, *Chem. Sci.* **2015**, *6*, 2474–2487.

- [44] J. England, E. Bill, T. Weyhermüller, F. Neese, M. Atanasov, K. Wieghardt, *Inorg. Chem.* **2015**, *54*, 12002–12018.
- [45] C. Wolff, A. Gottschlich, J. England, K. Wieghardt, W. Saak, D. Haase, R. Beckhaus, *Inorg. Chem.* **2015**, *54*, 4811–4820.
- [46] I. Mustieles Marín, T. Cheisson, R. Singh-Chauhan, C. Herrero, M. Cordier, C. Clavaguéra, G. Nocton, A. Auffrant, *Chem. Eur. J.* **2017**, *23*, 17940–17953.
- [47] C. S. Neumann, P. Fulde, *Z. Phys. B* **1989**, *74*, 277–278.
- [48] M. Dolg, P. Fulde, W. Kühle, C. S. Neumann, H. Stoll, *J. Chem. Phys.* **1991**, *94*, 3011–3017.
- [49] M. Dolg, P. Fulde, H. Stoll, H. Preuss, A. Chang, R. M. Pitzer, *Chem. Phys.* **1995**, *195*, 71–82.
- [50] C. H. Booth, M. D. Walter, D. Kazhdan, Y.-J. Hu, W. W. Lukens, E. D. Bauer, L. Maron, O. Eisenstein, R. A. Andersen, *J. Am. Chem. Soc.* **2009**, *131*, 6480–6491.
- [51] C. H. Booth, D. Kazhdan, E. L. Werkema, M. D. Walter, W. W. Lukens, E. D. Bauer, Y.-J. Hu, L. Maron, O. Eisenstein, M. Head-Gordon, R. A. Andersen, *J. Am. Chem. Soc.* **2010**, *132*, 17537–17549.
- [52] R. W. Field, *Ber. Bunsen-Ges.* **1982**, *86*, 771–779.
- [53] E. Schrödinger, *Ann. Phys.* **1926**, *384*, 361–376.
- [54] M. Born, R. Oppenheimer, *Ann. Phys.* **1927**, *389*, 457–484.
- [55] P. Hohenberg, W. Kohn, *Phys. Rev.* **1964**, *136*, B864–B871.
- [56] W. Kohn, L. J. Sham, *Phys. Rev.* **1965**, *140*, A1133–A1138.
- [57] P. G. Szalay, T. Müller, G. Gidofalvi, H. Lischka, R. Shepard, *Chem. Rev.* **2012**, *112*, 108–181.
- [58] J. W. Park, R. Al-Saadon, M. K. MacLeod, T. Shiozaki, B. Vlaisavljevich, *Chem. Rev.* **2020**, *120*, 5878–5909.
- [59] J. C. Slater, *Phys. Rev.* **1929**, *34*, 1293–1322.
- [60] E. U. Condon, *Phys. Rev.* **1930**, *36*, 1121–1133.
- [61] F. Coester, H. Kümmel, *Nucl. Phys.* **1960**, *17*, 477–485.
- [62] G. Das, A. C. Wahl, *J. Chem. Phys.* **1967**, *47*, 2934–2942.
- [63] P. Fulde, J. Keller, G. Zwignagl in *Solid State Physics, Vol. 41* (Eds.: H. Ehrenreich, D. Turnbull), Academic Press, Cambridge, MA, **1988**, pp. 1–150.
- [64] P. S. Riseborough, *Adv. Phys.* **2000**, *49*, 257–320.
- [65] A. Gilbert, N. S. Vidhyadhiraja, D. E. Logan, *J. Phys. Condens. Matter* **2007**, *19*, 106220.
- [66] G. Wilkinson, J. M. Birmingham, *J. Am. Chem. Soc.* **1954**, *76*, 6210.
- [67] J. M. Birmingham, G. Wilkinson, *J. Am. Chem. Soc.* **1956**, *78*, 42–44.
- [68] H. Schumann, J. A. Meese-Marktscheffel, L. Esser, *Chem. Rev.* **1995**, *95*, 865–986.
- [69] R. A. Andersen, J. M. Boncella, C. J. Burns, J. C. Green, D. Hohl, N. Rösch, *J. Chem. Soc. Chem. Commun.* **1986**, 405–407.
- [70] C. Benelli, D. Gatteschi, *Introduction to Molecular Magnetism: From Transition Metals to Lanthanides*, Wiley-VCH, Weinheim, **2015**, p. 71.
- [71] M. Tsutsui, T. Takino, D. Lorenz, *Z. Naturforsch.* **1966**, *21b*, 1–2.
- [72] S. Manastyrskij, M. Dubeck, *Inorg. Chem.* **1964**, *3*, 1647–1648.
- [73] O. Kahn, *Molecular Magnetism*, VCH, New York, N.Y., **1993**, pp. 31–52.
- [74] M. N. Bochkarev, L. N. Zakharov, G. S. Kalinina in *Organoderivatives of Rare Earth Elements*, Springer Netherlands, Dordrecht, **1995**, pp. 138–249.
- [75] M. Coreno, M. de Simone, J. C. Green, N. Kaltsoyannis, N. Narband, A. Sella, *Chem. Phys. Lett.* **2006**, *432*, 17–21.
- [76] R. Coates, M. Coreno, M. DeSimone, J. C. Green, N. Kaltsoyannis, A. Ker-ridge, N. Narband, A. Sella, *Dalton Trans.* **2009**, 5943–5953.
- [77] M. Coreno, M. de Simone, R. Coates, M. S. Denning, R. G. Denning, J. C. Green, C. Hunston, N. Kaltsoyannis, A. Sella, *Organometallics* **2010**, *29*, 4752–4755.
- [78] R. G. Denning, J. Harmer, J. C. Green, M. Irwin, *J. Am. Chem. Soc.* **2011**, *133*, 20644–20660.
- [79] M. Coreno, M. de Simone, J. C. Green, N. Kaltsoyannis, R. Coates, C. Hunston, N. Narband, A. Sella, *Dalton Trans.* **2014**, *43*, 5134–5141.
- [80] E. O. Fischer, H. Fischer, *J. Organomet. Chem.* **1965**, *3*, 181–187.
- [81] C. Calle, A. Sreekanth, M. V. Fedin, J. Forrer, I. Garcia-Rubio, I. A. Gromov, D. Hinderberger, B. Kasumaj, P. Léger, B. Mancosu, G. Mitrikas, M. G. Santangelo, S. Stoll, A. Schweiiger, R. Tschaggelar, J. Harmer, *Helv. Chim. Acta* **2006**, *89*, 2495–2521.
- [82] R. Pappalardo, C. K. Jørgensen, *J. Chem. Phys.* **1967**, *46*, 632–638.
- [83] C. J. Schlessener, A. B. Ellis, *Organometallics* **1983**, *2*, 529–534.
- [84] M. Schultz, J. M. Boncella, D. J. Berg, T. D. Tilley, R. A. Andersen, *Organometallics* **2002**, *21*, 460–472.
- [85] R. E. Da Re, C. J. Kuehl, M. G. Brown, R. C. Rocha, E. D. Bauer, K. D. John, D. E. Morris, A. P. Shreve, J. L. Sarrao, *Inorg. Chem.* **2003**, *42*, 5551–5559.
- [86] L. R. Morss, *Chem. Rev.* **1976**, *76*, 827–841.
- [87] F. Grandjean, G. J. Long in *Mössbauer Spectroscopy Applied to Inorganic Chemistry* (Eds.: G. J. Long, F. Grandjean), Springer US, Boston, **1989**, pp. 513–597.
- [88] G. Depaoli, U. Russo, G. Valle, F. Grandjean, A. F. Williams, G. J. Long, *J. Am. Chem. Soc.* **1994**, *116*, 5999–6000.
- [89] N. Kaltsoyannis, B. E. Bursten, *J. Organomet. Chem.* **1997**, *528*, 19–33.
- [90] Y. Baer, R. Hauger, C. Zürcher, M. Campagna, G. K. Wertheim, *Phys. Rev. B* **1978**, *18*, 4433–4439.
- [91] A. Franciosi, J. H. Weaver, N. Mårtensson, M. Croft, *Phys. Rev. B* **1981**, *24*, 3651–3654.
- [92] J. W. Allen, S. J. Oh, O. Gunnarsson, K. Schönhammer, M. B. Maple, M. S. Torikachvili, I. Lindau, *Adv. Phys.* **1986**, *35*, 275–316.
- [93] B. O. Roos, P. R. Taylor, P. E. M. Sigbahn, *Chem. Phys.* **1980**, *48*, 157–173.
- [94] K. Andersson, P.-Å. Malmqvist, B. O. Roos, A. J. Sadlej, K. Wolinski, *J. Phys. Chem.* **1990**, *94*, 5483–5488.
- [95] A. Greco, S. Cesca, W. Bertolini, *J. Organomet. Chem.* **1976**, *113*, 321–330.
- [96] A. Streitwieser, S. A. Kinsley, C. H. Jenson, J. T. Rigsbee, *Organometallics* **2004**, *23*, 5169–5175.
- [97] M. D. Walter, C. H. Booth, W. W. Lukens, R. A. Andersen, *Organometallics* **2009**, *28*, 698–707.
- [98] T. R. Bousie, D. C. Eisenberg, J. Rigsbee, A. Streitwieser, A. Zalkin, *Organometallics* **1991**, *10*, 1922–1928.
- [99] U. Kilimann, R. Herbst-Irmer, D. Stalke, F. T. Edelmann, *Angew. Chem. Int. Ed. Engl.* **1994**, *33*, 1618–1621; *Angew. Chem.* **1994**, *106*, 1684–1687.
- [100] K. O. Hodgson, K. N. Raymond, *Inorg. Chem.* **1972**, *11*, 3030–3035.
- [101] R. Shannon, *Acta Crystallogr. Sect. A* **1976**, *32*, 751–767.
- [102] A. Streitwieser, S. A. Kinsley, J. T. Rigsbee, I. L. Fragala, E. Ciliberto, *J. Am. Chem. Soc.* **1985**, *107*, 7786–7788.
- [103] H.-D. Amberger, H. Reddmann, F. T. Edelmann, *J. Organomet. Chem.* **2005**, *690*, 2238–2242.
- [104] N. M. Edelstein, P. G. Allen, J. J. Bucher, D. K. Shuh, C. D. Sofield, N. Kaltsoyannis, G. H. Maunder, M. R. Russo, A. Sella, *J. Am. Chem. Soc.* **1996**, *118*, 13115–13116.
- [105] C. H. Booth, M. D. Walter, M. Daniel, W. W. Lukens, R. A. Andersen, *Phys. Rev. Lett.* **2005**, *95*, 267202.
- [106] D. E. Smiles, E. R. Batista, C. H. Booth, D. L. Clark, J. M. Keith, S. A. Kozimor, R. L. Martin, S. G. Minasian, D. K. Shuh, S. C. E. Stieber, T. Tylicszak, *Chem. Sci.* **2020**, *11*, 2796–2809.
- [107] J. L. Sarrao, C. D. Immer, Z. Fisk, C. H. Booth, E. Figueroa, J. M. Lawrence, R. Modler, A. L. Cornelius, M. F. Hundley, G. H. Kwei, J. D. Thompson, F. Bridges, *Phys. Rev. B* **1999**, *59*, 6855–6866.
- [108] T. Vitova, K. O. Kvashnina, G. Nocton, G. Sukharina, M. A. Denecke, S. M. Butorin, M. Mazzanti, R. Caciuffo, A. Soldatov, T. Behrends, H. Geckeis, *Phys. Rev. B* **2010**, *82*, 235118.
- [109] M. W. Löble, J. M. Keith, A. B. Altman, S. C. E. Stieber, E. R. Batista, K. S. Boland, S. D. Conradson, D. L. Clark, J. Lezama Pacheco, S. A. Kozimor, R. L. Martin, S. G. Minasian, A. C. Olson, B. L. Scott, D. K. Shuh, T. Tylicszak, M. P. Wilkerson, R. A. Zehnder, *J. Am. Chem. Soc.* **2015**, *137*, 2506–2523.
- [110] A. B. Altman, J. I. Pacold, J. Wang, W. W. Lukens, S. G. Minasian, *Dalton Trans.* **2016**, *45*, 9948–9961.
- [111] S. G. Minasian, E. R. Batista, C. H. Booth, D. L. Clark, J. M. Keith, S. A. Kozimor, W. W. Lukens, R. L. Martin, D. K. Shuh, S. C. E. Stieber, T. Tylicszak, X.-d. Wen, *J. Am. Chem. Soc.* **2017**, *139*, 18052–18064.
- [112] A. Fujimori, *Phys. Rev. B* **1983**, *28*, 2281–2283.
- [113] A. Bianconi, A. Marcelli, H. Dexpert, R. Karnatak, A. Kotani, T. Jo, J. Petiau, *Phys. Rev. B* **1987**, *35*, 806–812.
- [114] A. Kotani, T. Jo, J. C. Parlebas, *Adv. Phys.* **1988**, *37*, 37–85.
- [115] G. Kaindl, G. Schmiester, E. V. Sampathkumaran, P. Wachter, *Phys. Rev. B* **1988**, *38*, 10174–10177.
- [116] M. V. Ganduglia-Pirovano, A. Hofmann, J. Sauer, *Surf. Sci. Rep.* **2007**, *62*, 219–270.
- [117] A. Kotani, H. Mizuta, T. Jo, J. C. Parlebas, *Solid State Commun.* **1985**, *53*, 805–810.

- [118] N. Hosoya, K. Yada, T. Masuda, E. Nakajo, S. Yabushita, A. Nakajima, *J. Phys. Chem. A* **2014**, *118*, 3051–3060.
- [119] N. Roesch, A. Streitwieser, *J. Am. Chem. Soc.* **1983**, *105*, 7237–7240.
- [120] M. Dolg, H. Stoll, *Theor. Chim. Acta* **1989**, *75*, 369–387.
- [121] M. Dolg, H. Stoll, H. Preuss, *J. Chem. Phys.* **1989**, *90*, 1730–1734.
- [122] W. Küchle, M. Dolg, H. Stoll, H. Preuss, *J. Chem. Phys.* **1994**, *100*, 7535–7542.
- [123] M. Dolg, X. Cao, *Chem. Rev.* **2012**, *112*, 403–480.
- [124] M. Dolg, P. Fulde, *Chem. Eur. J.* **1998**, *4*, 200–204.
- [125] A. Kerridge, R. Coates, N. Kaltsoyannis, *J. Phys. Chem. A* **2009**, *113*, 2896–2905.
- [126] R. F. W. Bader, *Atoms in Molecules: A Quantum Theory*, Clarendon Press, Oxford, **1994**, p. 438.
- [127] A. Kerridge, *Dalton Trans.* **2013**, *42*, 16428–16436.
- [128] O. Mooßen, M. Dolg, *Chem. Phys. Lett.* **2014**, *594*, 47–50.
- [129] A. Ashley, G. Balazs, A. Cowley, J. Green, C. H. Booth, D. O'Hare, *Chem. Commun.* **2007**, 1515–1517.
- [130] G. Balazs, F. G. N. Cloke, J. C. Green, R. M. Harker, A. Harrison, P. B. Hitchcock, C. N. Jardine, R. Walton, *Organometallics* **2007**, *26*, 3111–3119.
- [131] A. Kerridge, N. Kaltsoyannis, *C. R. Chimie* **2010**, *13*, 853–859.
- [132] M. Dolg, O. Mooßen, *J. Organomet. Chem.* **2015**, *794*, 17–22.
- [133] I. Hiroaki, S. Masahiko, *Chem. Lett.* **1992**, *21*, 147–150.
- [134] Y. Bian, J. Jiang, Y. Tao, M. T. M. Choi, R. Li, A. C. H. Ng, P. Zhu, N. Pan, X. Sun, D. P. Arnold, Z.-Y. Zhou, H.-W. Li, T. C. W. Mak, D. K. P. Ng, *J. Am. Chem. Soc.* **2003**, *125*, 12257–12267.
- [135] M. D. Walter, R. Fandos, R. A. Andersen, *New J. Chem.* **2006**, *30*, 1065–1070.
- [136] R. L. Halbach, G. Nocton, C. H. Booth, L. Maron, R. A. Andersen, *Inorg. Chem.* **2018**, *57*, 7290–7298.
- [137] R. L. Halbach, G. Nocton, C. H. Booth, L. Maron, R. A. Andersen, *Inorg. Chem.* **2018**, *57*, 8692.
- [138] P. L. Arnold, K. Wang, S. J. Gray, L. M. Moreau, C. H. Booth, M. Curcio, J. A. L. Wells, A. M. Z. Slawin, *Dalton Trans.* **2020**, *49*, 877–884.
- [139] N. T. Rice, J. Su, T. P. Gomba, D. R. Russo, J. Telsler, L. Palatinus, J. Bacsa, P. Yang, E. R. Batista, H. S. La Pierre, *Inorg. Chem.* **2019**, *58*, 5289–5304.
- [140] N. T. Rice, I. A. Popov, D. R. Russo, T. P. Gomba, A. Ramanathan, J. Bacsa, E. R. Batista, P. Yang, H. S. La Pierre, *Chem. Sci.* **2020**, *11*, 6149–6159.
- [141] L. M. Aguirre Quintana, N. Jiang, J. Bacsa, H. S. La Pierre, *Dalton Trans.* **2020**, *49*, 14908–14913.
- [142] M. D. Walter, M. Schultz, R. A. Andersen, *New J. Chem.* **2006**, *30*, 238–246.
- [143] M. D. Walter, D. J. Berg, R. A. Andersen, *Organometallics* **2006**, *25*, 3228–3237.
- [144] M. D. Walter, D. J. Berg, R. A. Andersen, *Organometallics* **2007**, *26*, 2296–2307.
- [145] G. Nocton, C. H. Booth, L. Maron, R. A. Andersen, *Organometallics* **2013**, *32*, 5305–5312.
- [146] G. Nocton, C. H. Booth, L. Maron, R. A. Andersen, *Organometallics* **2013**, *32*, 1150–1158.
- [147] G. Nocton, C. H. Booth, L. Maron, L. Ricard, R. A. Andersen, *Organometallics* **2014**, *33*, 6819–6829.
- [148] J. M. Veauthier, E. J. Schelter, C. J. Kuehl, A. E. Clark, B. L. Scott, D. E. Morris, R. L. Martin, J. D. Thompson, J. L. Kiplinger, K. D. John, *Inorg. Chem.* **2005**, *44*, 5911–5920.
- [149] C. N. Carlson, C. J. Kuehl, L. Ogallo, D. A. Shultz, J. D. Thompson, M. L. Kirk, R. L. Martin, K. D. John, D. E. Morris, *Organometallics* **2007**, *26*, 4234–4242.
- [150] I. L. Fedushkin, O. V. Maslova, E. V. Baranov, A. S. Shavyrin, *Inorg. Chem.* **2009**, *48*, 2355–2357.
- [151] I. L. Fedushkin, O. V. Maslova, A. G. Morozov, S. Dechert, S. Demeshko, F. Meyer, *Angew. Chem. Int. Ed.* **2012**, *51*, 10584–10587; *Angew. Chem.* **2012**, *124*, 10736–10739.
- [152] V. Goudy, A. Jaoul, M. Cordier, C. Clavaguéra, G. Nocton, *J. Am. Chem. Soc.* **2017**, *139*, 10633–10636.
- [153] M. Dolg, H. Stoll, H. Preuss, *Theor. Chim. Acta* **1993**, *85*, 441–450.
- [154] C. E. Kefalidis, L. Castro, A. Yahia, L. Perrin, L. Maron in *Computational Methods in Lanthanide and Actinide Chemistry* (Ed.: M. Dolg), **2015**, pp. 343–373.
- [155] A. A. Trifonov, T. V. Mahrova, L. Luconi, G. Giambastiani, D. M. Lyubov, A. V. Cherkasov, L. Sorace, E. Louyriac, L. Maron, K. A. Lyssenko, *Dalton Trans.* **2018**, *47*, 1566–1576.
- [156] N. A. G. Bandeira, C. Daniel, A. Trifonov, M. J. Calhorda, *Organometallics* **2012**, *31*, 4693–4700.
- [157] L. Jacquot, M. Xémard, C. Clavaguéra, G. Nocton, *Organometallics* **2014**, *33*, 4100–4106.
- [158] R. L. Halbach, G. Nocton, J. I. Amaro-Estrada, L. Maron, C. H. Booth, R. A. Andersen, *Inorg. Chem.* **2019**, *58*, 12083–12098.
- [159] C. V. Krishnan, C. Creutz, H. A. Schwarz, N. Sutin, *J. Am. Chem. Soc.* **1983**, *105*, 5617–5623.
- [160] H. Ferreira, M. M. Conradie, K. G. von Eschwege, J. Conradie, *Polyhedron* **2017**, *122*, 147–154.
- [161] A. Klein, W. Kaim, E. Waldhör, H.-D. Hausen, *J. Chem. Soc. Perkin Trans. 2* **1995**, 2121–2126.
- [162] W. W. Lukens, N. Magnani, C. H. Booth, *Inorg. Chem.* **2012**, *51*, 10105–10110.
- [163] J. D. Rinehart, M. Fang, W. J. Evans, J. R. Long, *Nat. Chem.* **2011**, *3*, 538–542.
- [164] J. D. Rinehart, M. Fang, W. J. Evans, J. R. Long, *J. Am. Chem. Soc.* **2011**, *133*, 14236–14239.
- [165] S. Demir, J. M. Zadrozny, M. Nippe, J. R. Long, *J. Am. Chem. Soc.* **2012**, *134*, 18546–18549.
- [166] C. A. Gould, L. E. Darago, M. I. Gonzalez, S. Demir, J. R. Long, *Angew. Chem. Int. Ed.* **2017**, *56*, 10103–10107; *Angew. Chem.* **2017**, *129*, 10237–10241.
- [167] D. Wang, J. Moutet, M. Tricoire, M. Cordier, G. Nocton, *Inorganics* **2019**, *7*, 58.
- [168] W.-H. Leung, Q.-F. Zhang, X.-Y. Yi, *Coord. Chem. Rev.* **2007**, *251*, 2266–2279.
- [169] L. Castro, Y.-M. So, C.-w. Cho, R. Lortz, K.-H. Wong, K. Wang, P. L. Arnold, K.-C. Au-Yeung, H. H.-Y. Sung, I. D. Williams, W.-H. Leung, L. Maron, *Chem. Eur. J.* **2019**, *25*, 10834–10839.

Manuscript received: October 27, 2020

Accepted manuscript online: December 19, 2020

Version of record online: February 25, 2021